# SYNTHESIS AND CHARACTERIZATION OF $MOS_2$ QUANTUM DOTS (QDS) ON P-SI SUBSTRATES FOR MULTIFUNCTIONAL OPTOELECTRONICS DEVICE APPLICATIONS

Thesis Submitted in Partial Fulfilment of the requirement for the Award of the Degree of

**Master of Engineering in Electronics & Telecommunication Engineering in Specialization of Electron Devices**

**of**

**JADAVPUR UNIVERSITY**

**by**


**ARPITA HOWLADAR**

**University Roll No. : 001710702019**

**Registration No. : 140703** of **2017-18**

**Examination Roll No. : M4ETC19021**

**Under the Supervision of**

**DR. DIVYA SOMVANSHI**

**&**

**PROF. SUBIR KUMAR SARKAR**

**Department of Electronics & Telecommunication Engineering**

**Jadavpur University, Kolkata-700032**

**West Bengal, India**


**MAY 2019**

**FACULTY OF ENGINEERING & TECHNOLOGY**

**JADAVPUR UNIVERSITY**

# CERTIFICATE OF EXAMINATION

This is to certify that the thesis entitled **"Synthesis and Characterization of $MoS_2$ Quantum Dots (QDs) on p-Si Substrates for Multifunctional Optoelectronics Device Applications"** has been carried out by **ARPITA HOWLADAR (Roll No: 001710702019, Examination Roll No: M4ETC19021 and Registration No: 140703 0f 2017-2018)** under my guidance and supervision and can be accepted in partial fulfilment for the degree of Master of Engineering in Electronics and Telecommunication Engineering in specialization of Electron Devices. In my opinion the work fulfils the requirement for which it is submitted. To the best of my knowledge, the matter embodied in the thesis has not been submitted to any other organization.

_____ _____

**Dr. Divya Somvanshi** **Prof. Subir Kumar Sarkar**

Joint supervisor

Department of Electronics and Tele-Communication Engineering

Jadavpur University, Kolkata – 700032

_____ _____

**Prof. Sheli Sinha Chaudhuri**

Head of the Department

Department of Electronics and

Tele-Communication Engineering

Jadavpur University, Kolkata – 700032

**Prof. Chiranjib Bhattacharjee**

Dean

Faculty Council of Engineering

and Technology (FET)

Jadavpur University, Kolkata – 700032

## FACULTY OF ENGINEERING & TECHNOLOGY

## JADAVPUR UNIVERSITY

### DEPARTMENT OF ELECTRONICS & TELECOMMUNICATION ENGINEERING

## CERTIFICATE OF APPROVAL*

The foregoing thesis is hereby approved as a credible study of an Engineering subject and presented in a manner satisfactory to warrant acceptance as pre-requisite to the degree for which it has been submitted. It is understood that by this approval the undersigned do not necessarily endorse or approve any statement made , opinion expressed or conclusion drawn therein but approve the thesis only for which it is submitted .

Committee on final examination
For the evaluation of the Thesis

BOARD OF EXAMINERS

---

(SIGNATURE OF THE EXAMINER)

---

(SIGNATURE OF THE SUPERVISOR)

*Only in case the thesis is approved.

# FACULTY OF ENGINEERING & TECHNOLOGY

# JADAVPUR UNIVERSITY

## DECLARATION OF ORAGINALITY AND COMPLIANCE OF ACADEMIC ETHICS

I the undersigned do hereby declare that this thesis contains literature survey and original work done by means a part of my **MASTER OF ENGINEERING IN ELECTRONICS AND TELECOMMUNICATION ENGINEERING IN SPECIALIZATION OF ELECTRON DEVICES.** All informations in this document have been obtained and presented in accordance with academic rules and ethical conduct. I also declare that as required by these rules and conduct I have fully cited and referenced all materials and results that are not original with this work.

**Name: ARPITA HOWLADAR**

**Examination Roll No. : M4ETC19021**

**Thesis Title: "Synthesis and Characterization of $MoS_2$ Quantum Dots (QDs) on p-Si Substrates for Multifunctional Optoelectronics Device Applications".**

**Date:**

_____

**Signature of the candidate**

# ACKNOWLEDGEMENTS

The success and final outcome of my thesis required a lot of guidance and assistance from many people and I am extremely fortunate to have got this all along the completion of my thesis work. Whatever I have done is only due to such guidance and assistance and I would not forget to thank them.

First and foremost, I owe my profound gratitude to my project supervisor, **Dr. Divya Somvanshi and Prof. Subir Kumar Sarkar** who guided me till the completion of my project work by providing his precious advices and constant support. I would like to express my special appreciation and thanks to him for giving his full effort in guiding me to maintain the progress. They have been a tremendous mentor for me because without his invaluable suggestions and his continued motivation, my project work would not have taken a worthwhile shape.

I am thankful to and fortunate enough to get such a nice support, devotion and constant encouragement from my senior, Ms. Sayantika Chowdhury, Mr. Anup Dey, throughout my thesis work. They supported me in guiding, inspired me to strive towards my goal.

I would not forget to remember all the members specially Mr.Ashoke Mondal, Mr.Rajib Samaddar, and Mr.Bikash Bhowmik of IC Centre, Department of Electronics and Telecommunication Engineering, Jadavpur University for their unlisted inspirations and insightful suggestions till my project work completed.

I would like to thank H.O.D Department of Electronics & Telecommunication Engineering, Jadavpur University by providing me all the facilities for carrying out the entire project work. I would like to express my sincere appreciation to all the teaching and non-teaching staff of the department for providing necessary support and aids.

Last but not the least, a special heartfelt thanks to my beloved family. Words cannot express how grateful I am to my parents for all of the sacrifices that they have made on my behalf. Their prayer for me was what sustained me thus far.

Date: _____

Place: Kolkata **Arpita Howladar**

**Synthesis and Characterization of $MoS_2$ Quantum Dots (QDs) on p-Si Substrates for Multifunctional Optoelectronics Device Applications**

# ABSTRACT

Two-dimensional (2D) transition metal dichalcogenide (2D-TMDC) semiconductors have attracted significant attention because of their unique physical properties which are very important for basic research and more device applications. Among all the 2D TMDC materials, Molybdenum disulfide ($MoS_2$) is one of the important candidates with direct band gap in monolayer form. It has unique excellent functional properties including high current carrying capacity and high carrier mobility. This has motivated several researchers to work in this area. $MoS_2$ QDs are used for different applications such as sensing and photo detection applications etc. In this thesis, I will discuss about the recent research advancement with emphasising on synthesis, optical and electrical characterization of $MoS_2$ QDs on p-Si substrate. Here, I have synthesised $MoS_2$ QDs by a facile colloidal method where ammonium tetrathiomolybdate $(NH4)_2MoS_4$) and oleylamine are used as a precursor and as a reducing agent, responding for prepare of $MoS_2$ QDs. The optical properties of prepared $MoS_2$ QDs have examined systematically by excitation dependent PL spectra and UV-Vis spectrum. The $MoS_2$ QDs/p-Si heterojunction diode observed by room temperature current-voltage (I-V) and Capacitance-voltage (C-V) characteristics. The lifetime of $MoS_2$ QDs have determined by time resolved PL spectra.

# CONTENTS

# LIST OF FIGURES

**Chapter 5**

# LIST OF TABLES

# LIST OF ABBREVIATIONS

| | |
|---|---|
| **TMDC** | Transition Metal Dichalcogenides |
| **$MoS_2$** | Molybdenum disulphide |
| **$MoSe_2$** | Molybdenum diselenide |
| **$WS_2$** | Tungsten disulfide |
| **$WSe_2$** | Tungsten diselenide |
| **QCE** | Quantum Confinement Effect |
| **QD** | Quantum Dot |
| **SEM** | Scanning Electron Microscopy |
| **PL** | Photoluminescence |
| **UV-Visible** | Ultraviolet-Visible |
| **I-V** | Current-Voltage |
| **C-V** | Capacitance-Voltage |
| **$(NH_4)_2MoS_4$** | Ammonium tetrathiomolybdate |
| **OA** | Oleic acid |
| **OLA** | Transition Metal Dichalcogenides |

# CHAPTER 1

# INTRODUCTION

## 1.1 Basic Overview:

The two-dimensional (2D) material refers to a group of materials which is weakly bonded by van-der Waals forces between layers. There is a large range of 2D materials included in this family named as Graphene, insulating hexagonal boron nitride (h-BN) and semiconducting transition metal dichalcogenides (TMDCs) materials[1-3]. Graphene was the first 2D material to be revealed in 2004 which is physically inaccessible by Andre Geim and Konstantin Novoselov at the University of Manchester, UK also awarded by Noble prize in Physics in 2010 [4, 5]. It has high mobility (approximately less than 10,000 $cm^2/Vs$), flexibility and strong mechanical properties. However, it is not appropriate for optoelectronics device application because it has zero band gap [6]. On the other hand, TMDCs are semiconductor materials having unique electronic and optoelectronic properties[7]. They have an indirect band gap in the bulk form whereas in monolayer it becomes direct band gap. These properties evolve from the quantum confinement effect (QCE) that arises due to thinning of materials at atomic level [3, 8].This varying band gap in TMDC is accompanied by a strong photoluminescence (PL) and large exciton binding energy[9]. TMDC materials are very important for basic research and simple device applications. TMDC materials having dangling-bond-free interfaces comparing to the traditional semiconductors. That is why it is making easy to combine TMDCs with different substrates. It is also use for a variety of opto-electronic devices, including solar cells, photo-detectors, light-emitting diodes, and photo-transistors. Due to the variety of properties owing to their broad-range of optical band gap variation with number of layers, efficient charge transfer and strong light-matter interactions; TMDC materials gives the basic substrates that allows creation of larger range of device for different applications.

## 1.2 Introduction to TMDC Materials

Transition metal dichalcogenides (TMDCs) materials constitute a very large class of materials. It is a combination of two elements, one is a transition metal atom (M) and another is a chalcogen atom (X). The chemical formula of TMDC material is $MX_2$, where M indicates a transition metal within the groups 4 to 10 of the periodic table and X indicates chalcogen elements from group 16 of the periodic table[10].Highlighted element in sky blue on the periodic table shown in Fig: 1.1indicates the transition element and dark yellow indicates chalcogen elements. Bulk TMDCs can be semiconductors such as $MoS_2$, $MoSe_2$, $WSe_2$, $WS_2$etc., semimetals such as $TiSe_2$,insulators such as $HfS_2$, or metals such as $TaS_2$ and $TaSe_2$ etc [11].

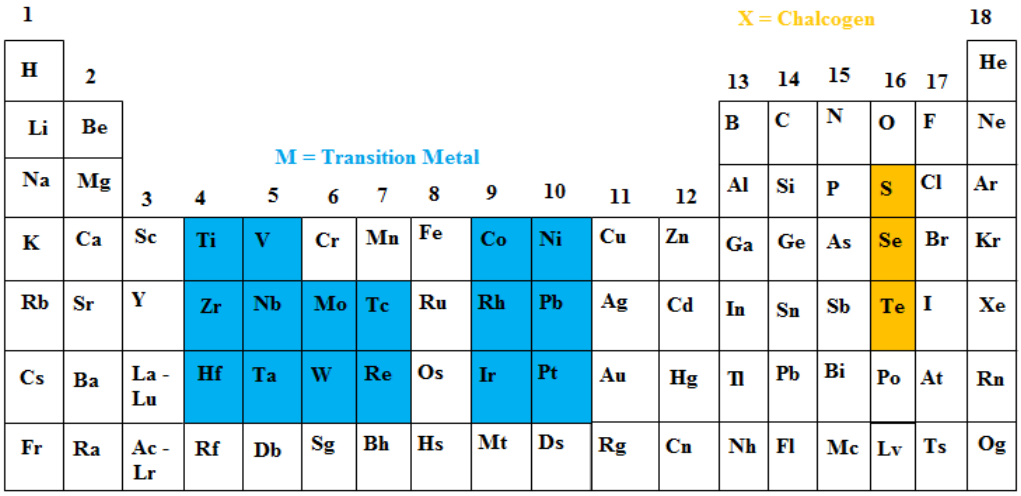


Fig: 1.1 Periodic table of elements presenting the possible combinations of elements forming layered TMDCs $MX_2$ [10]

Generally, TMDCs materials containing group 4-7 transition elements have a layered structure and group 8- 10 transition metals have non-layered structures [12]. In all bulk layered TMDCs; the stacked layers (X-M-X) are weakly bound by van der Waals forces [13, 14] and this weak interlayer bonds lead to easy intercalation of metals atoms between the layers. This intercalation is important for changes in the physical properties of the host compound[15].The weak interlayer bonding allow the bulk TMDCs for easily cleaved along the layer surface to form few layer or

single layer samples[16]. These layered structures are consists of hexagonal-packed transition metal atoms and they are inter layer between two layers of chalcogen. There is a tough interlayer covalent bonding between the metal (M) and the chalcogens (X). The possible co-ordinations adopted by the transition metal (M) of the TMDCs materials are either trigonal prismatic (H) or octahedral (T) [17].The crystal structures of TMDCs materials are existing 1T, 2H and 3R due to different stacking orders, or polytypes[18].

## 1.3 Molybdenum disulphide ($MoS_2$)

The chemical formula of Molybdenum disulfide is $MoS_2$. It is member of the group of TMDC materials. Molybdenum is a period 5 part and sulphur is a period 3 part.

### 1.3.1 Crystal Structure:

Among the TMDCs, $MoS_2$ is the most studied 2D material primarily because it is the most stable single layer TMDCs. It is also relatively easy to work with as it is abundantly available in bulk form. $MoS_2$ exist either as 2H or 1T phase [7, 19, 20]. In the 1T phase, the Mo-S coordination is octahedral, while in 2H phase, Mo-S coordination is trigonal prismatic. The 2H phase is a thermodynamically stable phase while 1T phases are metastable [17, 21].

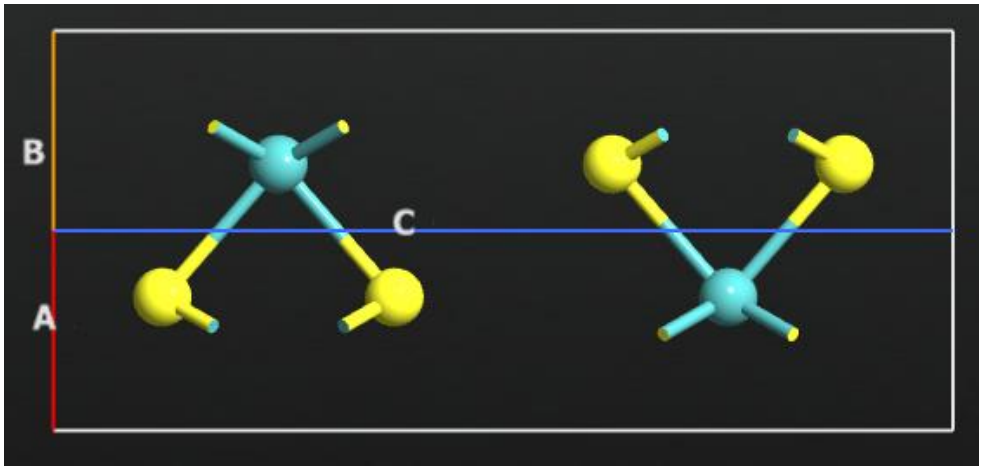


Fig: 1.2: Two single crystal of $MoS_2$ (TMDC materials)

Fig.1.2 shows two single crystal of hexagonal structure of $MoS_2$ drawn by Quantum ATK software. In this figure have one molybdenum (Mo) atom in bluish-green colour and two

disulfide (S) atoms in yellow colour. Fig.1.3 (a)-(d) shows that the layered structure of $MoS_2$ monolayer and bilayer (in 2D and 3D) formed by a hexagonal arrangement of Mo and S atoms stacked together. The S–Mo–S sandwiches are joined to each other by weak Van-der-Waals forces.

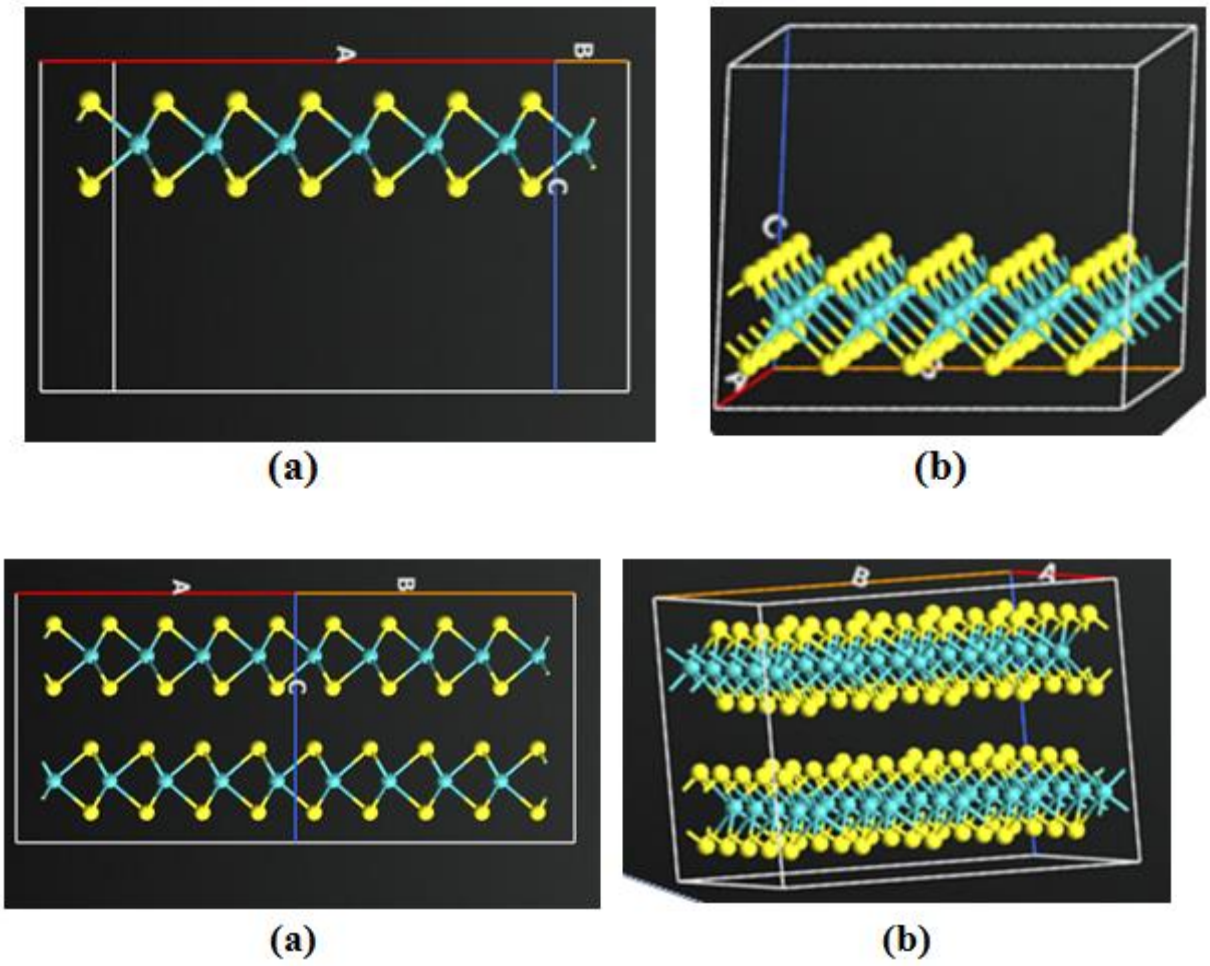


Fig.1.3: Schematic structure of  with the help of Quantum ATK software, showing M atoms are inter layer between two chalcogen (S atoms) planes viewed from the crystallographic direction (a) $MoS_2$ monolayer, in 1D and 3D (b) Bilayer $MoS_2$ structure in 1D and 3D.

### 1.3.2 Band Structure :

In general, the band gap ($E_g$) of any conventional semiconductor material is determined by energy difference between the valance band maximum (VBM) at the Γ point and the conduction band minimum (CBM) at the midpoint along Γ-k symmetry lines.$MoS_2$ exhibit 1.29 eV indirect band gap in the bulk form [3, 22], however the band gap changes from indirect to direct band gap of 1.9 eV [23] when bulk $MoS_2$ thinned down to a monolayer form, this is also verified experimentally as well as theoretically by many researchers [24]. It is known that the effect of quantum confinement (QCE) depends on the size, that is, the smaller the size, the greater the breadth of the forbidden zone due to the forbidden band [25]. The Bulk of TMDCs materials is an indirect forbidden zone with a valence band maximum (VBM) at the Γ point and a conduction band minimum (CBM) at the midpoint along Γ-K symmetry lines, while monolayer of TMDCs materials form is a direct band gap semiconductor with VBM and CBM coinciding at the K-point [26]. The band gap of TMDC materials varies for different materials, for example, direct band gaps of monolayer of $MoS_2$, $MoSe_2$, $WS_2$, and $WSe_2$, are estimated to be 1.88 eV, 1.57 eV, 2.03 eV, 1.67 eV respectively, whereas the indirect band gaps are 1.23 eV, 1.09 eV, 1.32 eV, and 1.21 eV respectively [20, 25, 27-31]. Here, the band structure of $MoS_2$ materials has stimulated by using Quantum ATK software (https://www.synopsys.com/silicon/quantumatk.html).

The band structures of the monolayer, bilayer, trilayer and 4 layer of $MoS_2$layers are analyzed by the density functional theory (DFT) using the Quantum ATK. In this DFT calculation, we have uses a numerical Linear Combination of Atomic Orbitals (LCAO). In the LDA calculations, we use k-point meshes of 14 × 14 × 7, 14 × 14 × 3, 14 × 14 × 14and 14 × 14 × 14 have been used in monolayer, bilayer, trilayer and 4-layer respectively [32-34].Using the DFT-LDA calculations. Fig: 6 show that the band structures monolayer, bilayer, trilayer and 4-layer of $MoS_2$ calculated at the DFT level. The green lines in horizontal indicate the Fermi level. The red colour of arrows indicates the fundamental band gap i.e. it may be direct or indirect for a given system. The base of the conduction band and peak of valence band are highlighted in black colour. Then we show that poly layers of $MoS_2$are indirect band gap semiconductors. The fundamental band gap initiates from transition from the base of conduction band halfway between Γand K points while the peak of valence band situated atΓ point. The optical direct band gap is situated at K point. As the number of layers decreases, the fundamental band gap increases that are why band gap is high in the monolayer and material changes into a 2D indirect to direct band gap semiconductor. The

band gap (Eg) of $MoS_2$ for monolayer 1.81 eV, for bilayer 0.807 eV, for trilayer 1.025 eV and for 4-layer 0.81 eV. The simulated band structures of $MoS_2$ are shown in the Fig.1 4.(a) ,(b), (c) and (d).

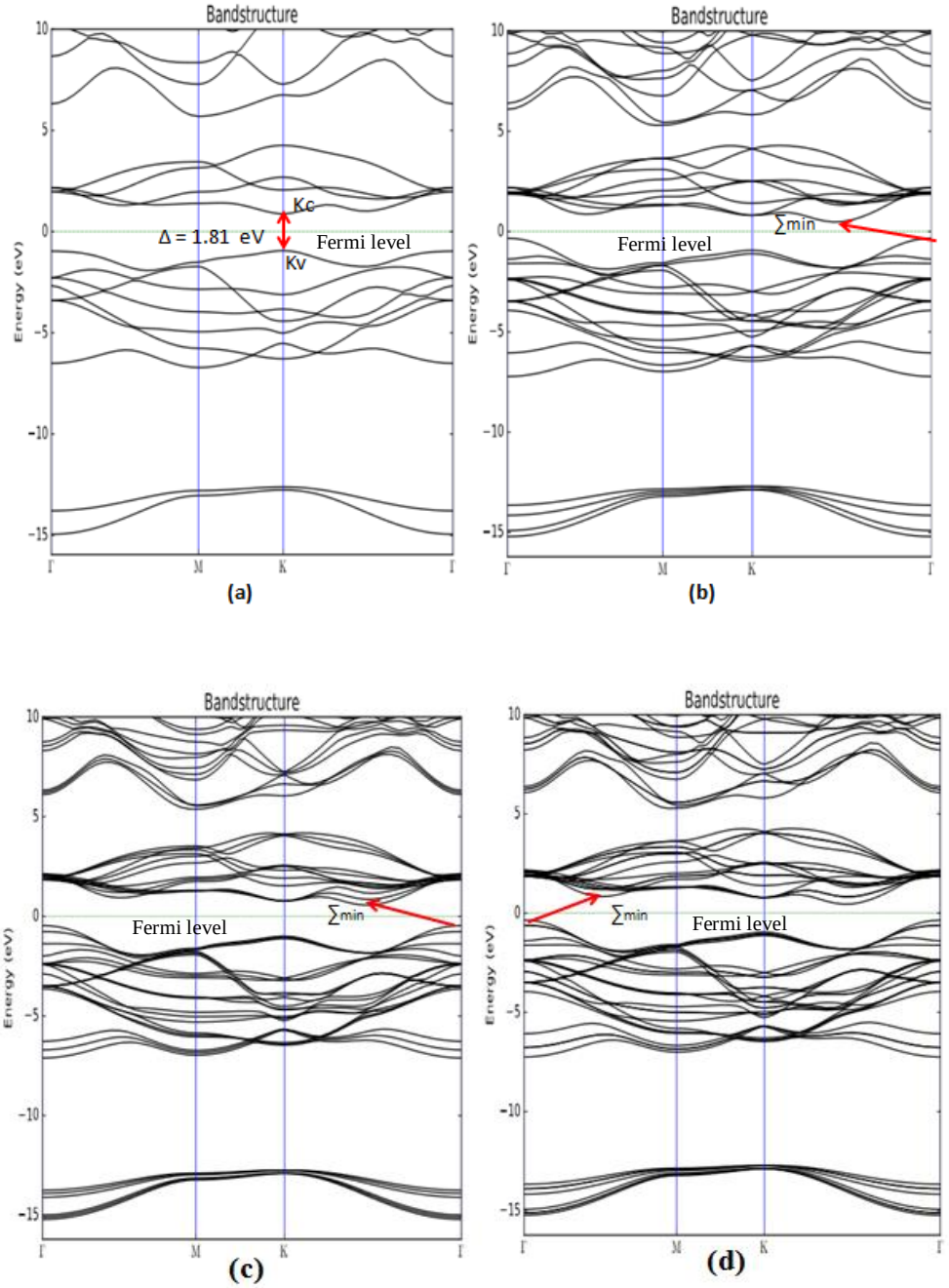


Fig.1.4: Band Structure of $MoS_2$ (a) Monolayer (b) Bi-layer (c) Tri-layer (d) 4-layer, simulated by using Quantum ATK. The solid light green line represents Fermi Level. The arrows indicate the fundamental band gap i.e. direct band gap or indirect band gap for a given system

**Table 1.1 of Band structure of $MoS_2$**

| **$MoS_2$ Structure** | **Transition point** | **Band gap** | |
|---|---|---|---|
| | | **Direct** | **Indirect** |
| Monolayer | $K_v$ to $K_c$ | 1.81 eV | |
| Bi-layer | $\Gamma$ to $\Sigma_{min}$ | | 0.807 eV |
| Tri-layer | $\Gamma$ to $\Sigma_{min}$ | | 1.025 eV |
| 4-layer | $\Gamma$ to $\Sigma_{min}$ | | 0.81 eV |

**Table.1.2 Physical Properties of $MoS_2$**

| **Property** | **Value** |
|---|---|
| Molecular Formula | $MoS_2$ |
| Apperance | black/lead-gray solid |
| Melting point | 1185 °C |
| Boiling point | 2375 °C |
| Solubility in water | Insoluble |
| Lattice parameters at 300 K | $a_0$ = 0.3161 nm (2H), 0.3163 nm (3R), $c_0$ = 1.2295 nm (2H), 1.837 (3R) |
| Density | 5.06 g/cm$^3$ |
| Thermal conductivity | 155 W/mK to 115 W/mK |
| Energy bandgap | 1.8 eV Direct (monolayer),1.23 eV Indirect (Bulk) |
| Exciton binding energy | 240 meV |
| Electron effectve mass | $0.45\, m_0$ |
| Electron Hall mobility at 300K | 200 cm$^2$ V$^{-1}$ s$^{-1}$ |
| Hole effective mass | $0.43\, m_0$ |

## 1.4 Quantum Confinement Effect:

Quantum confinement effect (QCE) is observed in a material when size of the material is very small as compared to the de-Broglie wave length of electron[8, 35, 36] The ranges of quantum confinement from 1 to 25 nm for usual semiconductors belongs to groups of IV, III-V and II-VI[37]. Electrons sense the presence of the particle boundaries and react to changes in particle size, regulating their energy due to the limitation. This thing is known as a quantum-size effect. The particle size of a semiconductor is near and below the bulk exciton the Bohr radius of a semiconductor when QCE dominates. The equation of the Bohr radius is [36]

$$a_B = \varepsilon \frac{m_0}{m^*} a_0 \tag{1.1}$$

Where, m* is the mass of the particle, ε is the dielectric constant of the material, $a_0$ is the Bohr radius of the hydrogen atom, and $m_0$ is the rest mass of the electron. When the particle size approaches the Bohr radius, the exciton leads to an increase in the energy of the exciton transition [36]. In addition, quantum confinement tends to the breakdown of the continuous energy zones of bulk material into discrete atomic approximating energy levels. Fig. 1.5 shows the discrete absorption spectrum of energy states. A quantum bounded structure is a structure in which the motion of the carriers i.e. electron and hole is limited in all directions by potential barriers[36]. Based on the direction of confinement, a quantum bounded structure will be classified into three categories and classified as quantum well, quantum wire and quantum dots or nanocrystals [36]. Table.1.3 shows that this is the main type of quantum bounded structure

**Table 1.3: Classification of quantum confined structures**

| Structure | Quantum confinement | Number of free dimension |
|---|---|---|
| Bulk | 0 | 3 |
| Quantum well/superlattices | 1 | 2 |
| Quantum wire | 2 | 1 |
| Quantum dot/Nanocrystals | 3 | 0 |

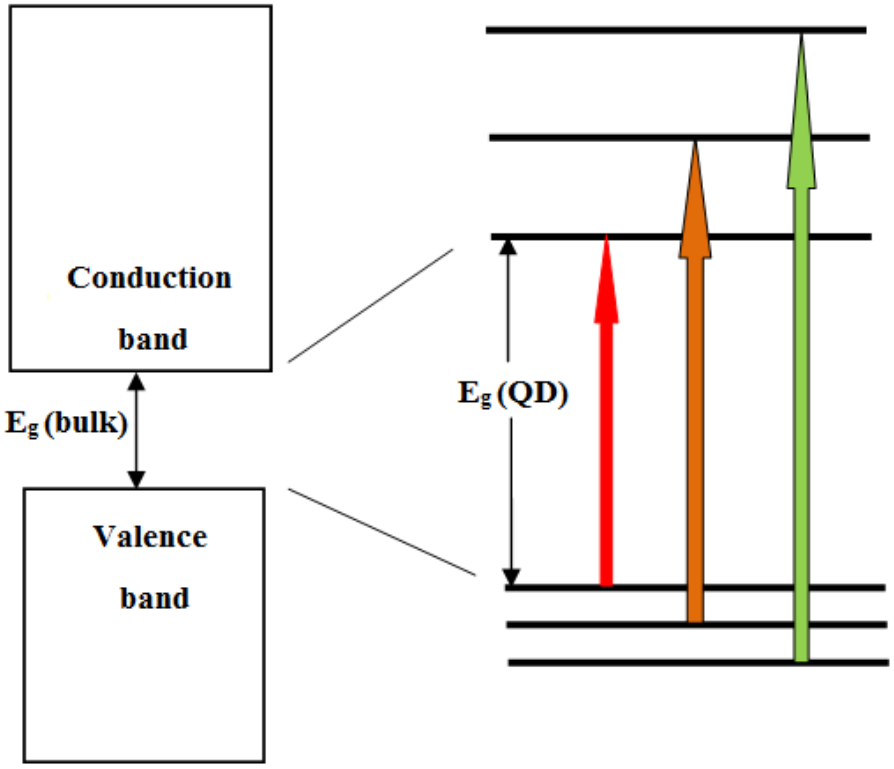


Fig. 1.5: A schematic structure of the discrete energy level of a semiconductor.

Quantum dots are semiconductor nanoparticle where charge carriers are confined in all x, y, z dimensions and it is a tiny zero-dimensional or low dimensional [38] size in the range of nanometers, so it name is **dot** [39]. Quantum Dots (QDs) are very small semiconductor nanoparticles that range from 2-10 nm diameters. It has unique optical and electrical properties. Electronics characteristics of Quantum Dots (QDs) related to the size and shape of the individual crystals [39]. Due to each quantum dot is a small semiconductor, QDs glow a particular colour after illuminated by light. The glow of colour depends on the size of nanoparticles. For larger nanoparticles i.e. energy difference between conduction band and valance band is higher, so emit longer wavelengths like red, while smaller nanoparticles i.e. energy difference between valance band and conduction band is lower, so emit shorter wavelengths like blue. QDs are not only determined by it size but also by its shape, structure and material construction and the dependence on size arises from changes of the surface-to-volume ratio with size, and from quantum confinement effects [40].

When the location of a particle (for example holes and electrons) is confined to a region of space, quantum confinement arises. This is the idea behind the "Particle in a Box" system-

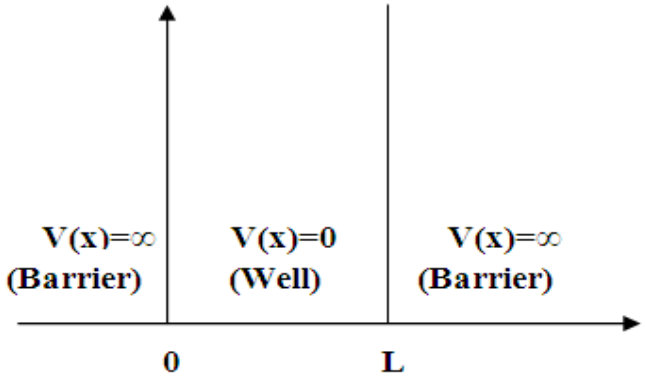


The walls of a one-dimensional box fill with an infinitely large potential energy when visualized as area of space. . On the other hand, if it touches the walls of the box, preventing it exit due to the infinitely large forces, repel the particle. In this model the potential energy is given as

$$V(x)=\begin{cases}0, 0<x<L\\ \infty, otherwise\end{cases} \qquad (1.2)$$

Where ***x*** is the position within the box and L is the length.

In quantum mechanics, the wave function gives the most fundamental description of the behavior of a particle. The wave function can be found by solving the Schrödinger equation for the system i.e. the equation is

$$\psi(x,t)=[A\sin(kx)+B\cos(kx)]e^{-iwt} \qquad (1.3)$$

Now we apply the boundary condition that

$$\psi(0)=\psi(L)=0 \qquad (1.4)$$

Then we get,

$$\psi(x)=\sqrt{2/L}\sin(\frac{n\pi x}{L}) \qquad (1.5)$$

Where n=1, 2, 3…….

We know for the free particle, when V(x) =0, we get

$$E\psi(x) = \frac{-\hbar^2}{2m}\frac{d^2}{dx^2}\Psi(x) \tag{1.6}$$

After the calculation we get,

$$E_n = \frac{n^2\hbar^2}{8mL^2} \tag{1.7}$$

Due to quantum confinement, the radius of the Quantum Dot influence the wavelength of the emitted light and the effect of a change of the radius of the quantum dot on the wavelength λ of the emitted light, this is describes by this equation because E = hc / λ, where c is the speed of light. This is help for the calculating the radius of a quantum dot with the parameters experimentally determined. So the general equation is,

$$\Delta E(r) = E_{gap} + \frac{h^2}{8r^2}(1/m_e^* + 1/m_h^*) \tag{1.8}$$

Where, r is the radius of quantum dots, $m_e^*$ and $m_h^*$ are effective mass of electron and hole respectively, $E_{gap}$ is the energy gap of the band.

QDs have many advantages that are why it has many applications. For example, They are used in television industry due to ultra-high definition colours and increased effective viewing angles and they are also used in solar cell making due to increase in efficiency. Quantum Dots can also be used for producing images of cancer tumours.

## 1.5 Characterization Techniques :

In this section, the different technique used in this work for characterization of materials will be discussed in details.

### 1.5.1 Scanning Electron Microscopy (SEM)

The scanning electron microscope (SEM) is a type of electron microscope that builds up the images of the sample's surface point by point in a time sequence by scanning it with a high-energy beam of electrons. The electrons interact with the atoms that make up the sample and

produce signals containing the information about the sample's surface topography and composition. A field emission SEM (FESEM) is a type of SEM where a field-emission cathode in the electron gun of a SEM provides narrower probing beams at low currents as well as high electron energy, resulting in both improved spatial resolution and minimized sample charging, and damage. It is used for applications which demand the highest magnification possible. When high energy electrons impose on the surface of a sample, a number of signals are generated:

1. ● Backscattered electrons –high energy electrons which are scattered out of the specimen, losing only a small amount of energy.
2. ● Secondary electrons – this kind of electron originate in the specimen itself, and have a much lower energy than the backscattered electrons.
3. ● X-rays - theses electron give information about the elemental composition of the sample.

To obtain an image in the SEM, some variation in the signal from different parts of the sample must be taken. The resolution of the SEM is determined by the size of the incident beam. The yield of secondary electrons is at a minimum when the surface of the specimen is perpendicular to the electron beam. At regions of the specimen which are not exactly perpendicular to the beam, electrons are more likely to be scattered out of the specimen, rather than further into the specimen. Hence, such regions appear bright in the secondary electron image. Astigmatism is a problem that is commonly encountered in SEM. The effect of astigmatism is that objects in the image generally appear “stretched” in one direction, and then in the other direction. All electron microscopes are equipped with stigmators, which allow the user to correct the astigmatism.

### 1.5.2 Photoluminescence (PL) :

Photoluminescence (PL) spectroscopy is a powerful method for analyzing the electronic structure of semiconductor and semi-insulating materials. The electrons are jump to a higher electronic state (valance band to conduction band) due to photo-excitation after that it will relaxes and release the energy in the form of light and returns to back to a lower energy level i.e. conduction band to valance band (shows in Fig: 1.6). Photoluminescence Spectroscopy uses a laser beam for capturing the light which is generated from a material. When it is irradiated by a laser beam, it jumps from the excited state to ground state . Material imperfections and impurities both are necessity for measuring the luminescence spectrum. For the transition probability, every excited

atom will get de-excited to several other lower levels and each transition we can get different peaks. PL has many other methods and they are more useful for fundamental scientific research. All these methods are more complex than the PL spectra [41].

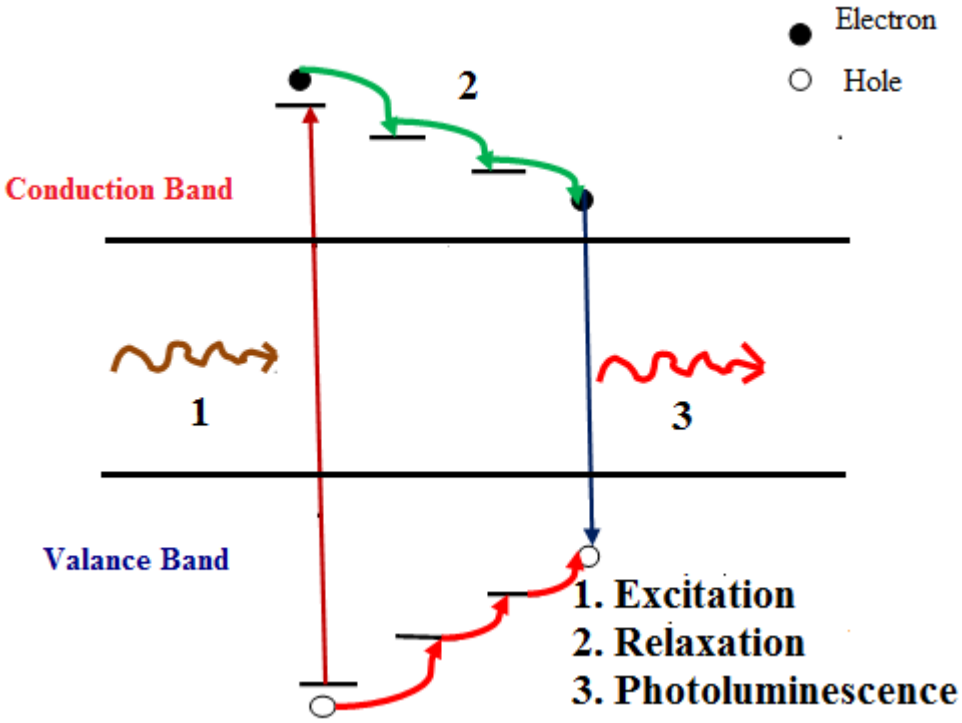


Fig.1.6: structural diagrams of Excitation, Relaxation and Photoluminescence

### 1.5.3 Raman Spectra :

The Raman Effect was discovered in 1928 by C.V. Raman and K.S. Krishnan is a recognized tool for observing vibrational, rotational, and other low-frequency modes in materials as well as providing a structural fingerprint with which molecules can be identified. It is based on inelastic scattering of a photon by molecules. This can happen with a change in the vibrational, rotational or electronic energy of a molecule.Fig.1.7 shows that condition of Raman scattering of light by molecules. Raman spectroscopy is a vibrational spectroscopic technique; it is provide the information about chemical structure, phase and polymorphism, intrinsic stress/strain, contamination and impurity of sample. Sample may be in the form of Solids i.e. particles, pellets,

powers, films, fibres, Liquids i.e. gels, pastes and Gases. I can identify the material using Raman shifts. As a rule of sample is illuminated by a laser beam. Electromagnetic radiation from the illuminated spot is together by the lens and pass through the monochromator. Variations in spectra depend on the position on the sample. This variation gives the information about the homogeneity of the material. It has some unique advantages such as Non-contact and non-destructive analysis, High spatial resolution up to sub-micron scale, it is possible to measure both organic and inorganic substances, Samples will be various states and works on Low dimensional materials. For these advantages, it is used for verity of field.

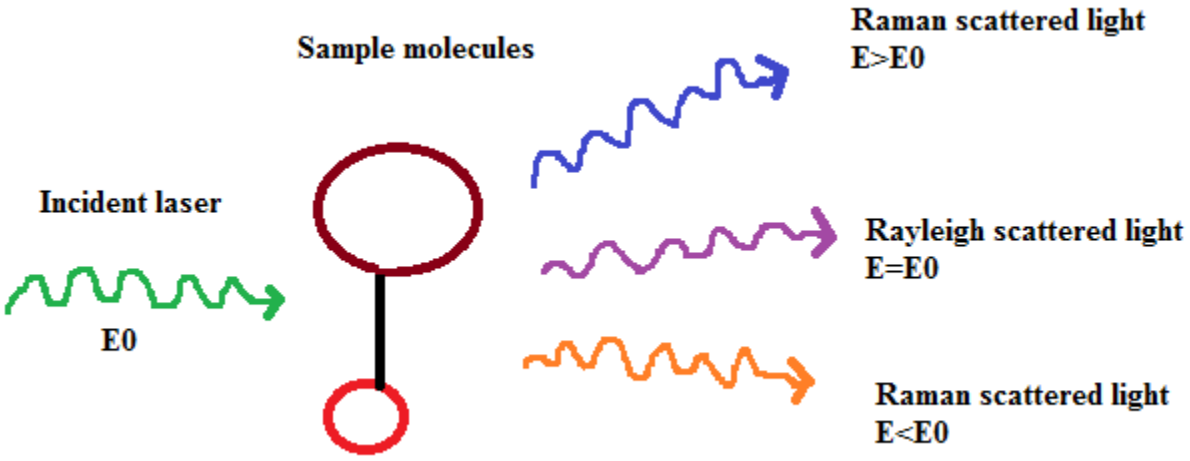


Fig.1.7 Raman scattering of light by molecules

### 1.5.4 UV-Visible Spectroscopy :

Ultraviolet-visible (UV-Vis) spectroscopy is also popular analytical techniques in the laboratory. Founder of eponymous company, Arnold Beckman, introduced this UV-vis spectrophotometer in July 1941. In UV-Vis spectroscopy, light is passed through a sample at a specific wavelength in the UV or visible spectrum. The sample not all of the light will be transmitted, it absorbs some of the light. The absorbance can be used to obtain the concentration of a sample. It can also be used to identify a compound by comparing the measured optical density in the wavelength range. This is called the absorbance spectrum. The wavelength of the ultraviolet region and visible region is in the range between 190-380 nm and 380-750 nm, respectively. Each molecules have unique absorbance spectra due to the chemical structure determines the band gap. When a photon hits a

molecule and is absorbed, the molecule is jumped from ground state to a higher energy state. The energy difference between the two states is called the band gap. The energy of the photon must be equal to the band gap in order for the photon to be absorbed. Absorbance follows the principle of Beer's Law.

Measuring instruments and the operation of the UV spectrometers can be considered and latest modern UV spectrometers consist of Light source, Monochromator, Sample and reference cells, Detector, Amplifier, Recording devices.

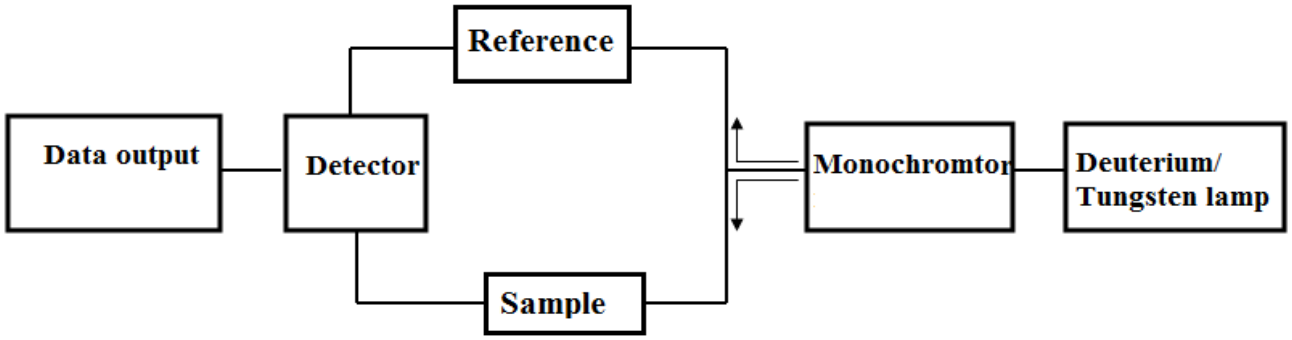


Fig. 1.8: Block Diagram of UV -visible Spectrometer

This Spectroscopy calculated the maximum wavelength. When we scan a sample using the ultra violet rays, it absorbs the UV rays and gives a wide spectrum. This means that the sample absorbs all the various wavelengths of the UV rays. It is absorbed by the each wavelength absorbed and at a particular wavelength, absorption is Maximum. Where the absorption is maximum, there is also wavelength is maximum.

This spectroscopy has some advantages such as Fast sample analysis, Suitable for a broad different of analyses, much easier than chromatographic techniques, User-friendly interface and little maintenance required. For these reasons, it is used to verity of field like that research field, biological field etc. But this spectroscopy has some limitations like as relatively low sensitivity, temperature changes; other sample components are not identify as chromatography, requires a relatively large sample volume etc.

## 1.6 Motivation of Thesis:

TMDC quantum dots (QDs) are of fundamental interest due to a stronger quantum size effect with reduced lateral dimensions. In recent times, TMDCs have received a notable amount of

interest due to their attractive properties and adaptable potential applications. They were used to study quantum phenomena due to their exclusive band structures and new electronic properties. $MoS_2$ is a type of TMDC material and it has become an important candidate of 2D materials. When 2D $MoS_2$ materials reduced to zero dimensional or low dimensional then the new optical properties emerges. That is why it points to quite a lot of potential technological advantages in electronic, magnetic, optical, and catalytic properties. It has also high current-carrying capacity and large carrier mobility. In QDs, electrons are limited in all lateral dimensions, which allow for detailed study and control manipulations with individual quantum systems. From literature review, it is observed that the electrical properties of $MoS_2$ QDs and Si based heterojunction diode have not explored in details. Therefore, the basic objective of present thesis is to investigate the electrical characteristics of $MoS_2$ QDs based thin film grown on p-Si substrates for electronic and optoelectronics applications.

## 1.7 Organisation of the Thesis:

The basic objective of present thesis is to synthesis n-$MoS_2$ QDs on p-Si substrates with facile-colloidal approach and investigate electrical characteristics of n-$MoS_2$/p-Si heterojunction diodes (for their compatibility with CMOS technology) for electronic and optoelectronics applications. The present dissertation consists of six chapters including the present one entitled as "Introduction". The contents of chapters are as follows:

**Chapter-1** discuss about the introduction of the TMDC materials and details about Molybdenum disulphide ($MoS_2$). The crystal structure and band structure of $MoS_2$ (monolayer, bilayer, tri-layer and Quad-layer) have been analyzed with DFT theory by using Quantum ATK software. The basic details about Quantum confinement effect has discussed. The working principle of some characterization techniques such as Scanning Electron Microscopy, Photoluminescence spectra and UV-Visible spectroscopy have been discussed in details.

**Chapter-2** includes the literature review of some of the major state-of-the-art-research works in the related area of n-$MoS_2$/p-Si based devices. Based on the literature survey and keeping in the view of various lacunas, the motivation behind the present study is outlines at the end of this chapter.

**Chapter-3** begins with the discussion on the introduction of Heterostructure, different type of heterostructures and energy band diagram of $MoS_2$/p-Si heterojunction diode before and after thermal equilibrium. The basic mechanism of current transport process by using thermionic emission theory explained in details.

**Chapter-4** discusses the synthesis of $MoS_2$ QDs by facile –colloidal synthesis method. The characterization of $MoS_2$ QDs have been determined by SEM images, Excitation dependent PL spectra and UV-Visible spectrum. The band gap of MoS2 has been calculated by UV-Vis spectrum.

**Chapter-5** is devoted to the electrical characteristics of n-$MoS_2$/p-Si heterojunction diodes by Current –voltage (I-V) and capacitance-voltage (C-V) characteristics, and time-resolved PL (TRPL) measurement. The donor concentration of $MoS_2$ thin film has been calculated by room temperature C-V characteristics. The values of electrical parameters such as barrier height, and Ideality factor have been determined from the measured room temperature I-V characteristics. The life-time of MoS2 QDs has been determined by TRPL spectroscopy.

**Chapter-6** summarizes some major outcomes and finding of the thesis. This chapter has been devoted to conclude the major findings from the discussions of the previous chapters of the present thesis.

# CHAPTER 2

# LITERATURE REVIEW

## 2.1 Introduction:

One of the main functional characteristic of QDs is absorbs photons of light and the re-emit the light which can be tuned simply by varying their size, since QDs with different sizes having different band gaps, they can absorb and emit different frequencies [42]. Thus, the size tunable absorption and luminescence spectra of QDs stem from the quantum confinement effect. In addition, the investigation of how the quantum mechanical effect changes the geometry (i.e. formation energy) and electronic characteristics (charge density, spin density, etc.), 2D $MoS_2$ sheets transform to quantum dot as reported by Loh et al. [43]. It was inferred that the bonding between the Mo atoms in monolayer QDs was stronger than that in the monolayer sheet. The properties of $MoS_2$ QDs are mainly based on the edge structure and shapes. Pei *et al.*[44] has systematically explored the structural stability, electronic and magnetic properties of different $MoS_2$ QDs based on first principles with the different chemical potentials of sulphur.

## 2.2 Literature Review:

In 2014, Wang *et. al*. [45] demonstrate "*Molybdenum Disulfide Quantum Dots as a Photoluminescence Sensing Platform for 2,4,6-Trinitrophenol Detection*". In this paper author reported the synthesis of photo luminescent $MoS_2$ materials and their applications in analytical chemistry. The prepared $MoS_2$-QDs were characterized by transmission electron microscopy (TEM), atomic force microscopy (AFM), X-ray photoelectron spectroscopy, Fourier transform infrared spectroscopy, photoluminescence spectroscopy (PL), and UV–vis spectroscopy. In 2015, Lin *et. al*. [46]demonstrate "*Colloidal synthesis of $MoS_2$ quantum dots: size-dependent tunable photoluminescence and bioimaging*". In this article, the author reported that photoluminescent

$MoS_2$-QDs were obtained by ammonium tetrathiomolybdate ($(NH_4)_2MoS_4$) and oleyl amine as a precursor and as a reducing agent. The optical properties and structure of freshly prepared $MoS_2$-QDs were characterized by the methods of transmission electron microscopy (TEM), photoluminescence spectroscopy (PL), Raman spectroscopy, X-ray diffraction (XRD). After analyzing the results confirmed that a fluorescent signal appears in the cytoplasm which indicates that the finished $MoS_2$-QDs could be used as a probe for optical cell visualization in real time. In 2016, Mukherjee *et. al.* [47] demonstrate "*Novel Colloidal $MoS_2$ Quantum Dot Heterojunctions on Silicon Platforms for Multifunctional Optoelectronic Devices*". In this article, the author reported that a Silicon wafer scale $MoS_2$ heterojunction diode for the first time uses colloidal quantum dots. The Size dependent rectilinear emission of $MoS_2$ dots in presented at room temperature. Fabricated n-$MoS_2$/P-Si heterojunction are manufactured and excellent results were obtained after analysis. After that the author came to the conclusion that a large area photo detector made using two dimensional materials. In 2017, Li *et. al.*[48] demonstrate "*Preparation of Monolayer $MoS_2$ Quantum Dots using Temporally Shaped Femtosecond Laser Ablation of Bulk $MoS_2$ Targets in Water.* The as-prepared $MoS_2$-QDs were characterized with the transmission electron microscopy (TEM), X-ray diffraction (XRD), Raman spectroscopy, X-ray photoelectron spectroscopy, UV–vis absorption spectra, and photoluminescence spectra (PL) for analysis the morphology, crystal structures, chemical, and optical properties. The analysis results show that monolayer $MoS_2$-QDs can be successfully prepared. The as-prepared $MoS_2$-QDs exhibit excellent electro catalytic activity for hydrogen evolution reactions due to the high specific surface area, and excellent electrical conductivity. In 2019,Veeramalai *et. al.*[49]demonstrate "*Highly flexible memristive devices based on $MoS_2$ quantum dots sandwiched between PMSSQ layers*". In article reports that an easy, cost effective method that uses the hydrothermal water process for the synthesis of two-dimensional $MoS_2$-QDs. These are applications in flexible memristive devices. The PL and time-resolved PL spectra of the $MoS_2$-QDs a strong radiation in the blue region with a slower damping constant. As fabricated device exhibits high ON–OFF current ratio, stable retention, and excellent endurance in the relaxed state. These analyzes noticeably show that ultrathin two-dimensional QDs are using high-performance flexible memristive devices.

# CHAPTER 3

# HETEROSTRUCTURE BASED ON $MoS_2$/p-Si

## 3.1 Introduction to Heterostructures :

A heterostructure is a sandwich structure of material layers of dissimilar crystalline semiconductors with unequal band gaps. Semiconductor heterostructures have been used for variety of application which includes laser diodes, light emitting diodes, optical detectors, and solar cells etc. [50]. In general, structures of heterostructure mainly utilize III–V and IV–VI compounds due to similar crystal structures and closely matched lattice constants which is essential and necessary condition for heterostructure formation. If the lattice mismatching occurred between the participating semiconductors, the crystalline defects are occurred. Heterostructures with good crystalline interfaces have been grown using few binary materials, the examples are GaAs/AlAs, InAs/GaSb, InAs/AlSb and InSb/CdTe. It can be mentioned here that the lattice constants of GaAs and AlAs are almost equal, therefore these materials are quite well combined with each other, as $Al_xGa_{1-x}As$ exists for all x such that $0 \leq x \leq 1$ [51].For heterostructures devices based on nanostructures materials, sharp junction is required, since for quantization the dimensions are required is order of electron wavelength. The Nobel Prize in physics in 2000 was awarded to H. Kroemer of the University of California, USA and Z. I. Alferov of Ioffe Institute, Saint Petersburg, Russia for developing semiconductor heterostructures.

## 3.2 Different type of Heterostructures :

The first successful heterojunction structure of Ge/GaAs was developed by Anderson in 1960 [52]. He developed the well-known Anderson model [52] to determine the energy band diagram

of heterojunctions at the interface for prediction of the current flow. The model [52] was based on the assumption of the ideal heterojunctions where the interface states are assumed to be zero at the interface and current transport is assumed to be entirely by injection of carriers over the band offsets into the quasi-neutral region of the semiconductors. The Anderson model [52] is generally used for studying theoretical performance of the ideal heterojunctions.

Heterostructures are classified according to the alignment of valance band and conduction band of the two semiconductors. There are three types of different alignments namely,

(i) Type I or Straddled alignment,

(ii) Type II or Staggered alignment,

(iii) Type III or Broken gap alignment.

### 3.2.1 Type I or Straddled alignment :

When the band gap of one material totally overlaps to the other band gap of material, the narrower band gap is enclosed within the wider band gap. In this case, $E_{V1}>E_{V2}$ and $E_{C2}>E_{C1}$ and the signs of band offsets for the two bands are opposite. E.g. GaAs/AlGaAs, GaSb/AlSb, GaAs/GaP.Type I band alignment shows in fig. 3.1.

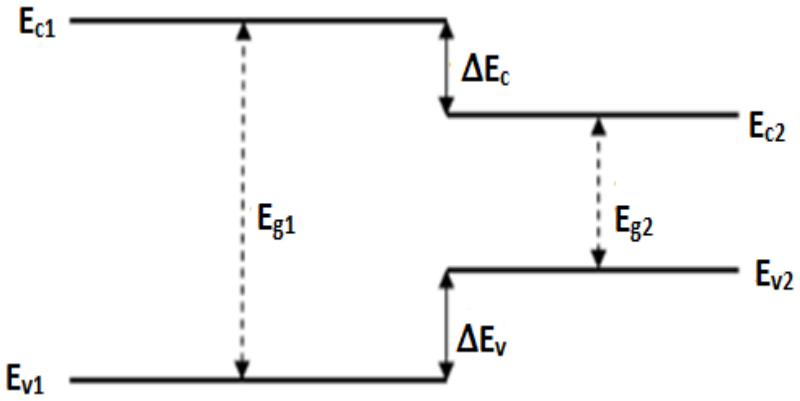


Fig. 3.1Type 1Straddled alignment

### 3.2.2 Type II or Staggered alignment :

The band gap of one semiconductor material entirely overlaps to the other band gap of material with $E_{V1}>E_{V2}$, $E_{C1}>E_{C2}$ and $\Delta E_C<E_{g1}$. In this case, the band offsets have the same sign. Both the conduction band edge and valance band edge of one material being lower than the equivalent

band edges of other material. E.g. InP/AlInP, InGaAs/GaSbAs and AlInAs/InP. Type II band alignment shows in fig. 3.2.

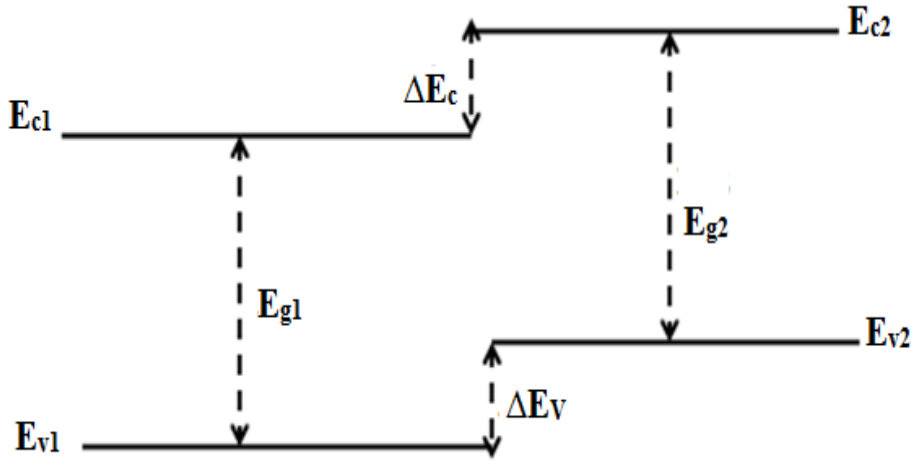


Fig. 3.2 Type II Staggered alignment

### 3.2.3 Type III or Broken gap alignment :

The band gap of one material do not overlaps to the other band gap of material because $E_{V2}>E_{V1}$, $E_{C2}>E_{C1}$ and $\Delta E_C>E_{g1}$. In this case, the band offsets have the same sign [53]. Both the conduction band edge and valance band edge of one material being separately lower than the band edges of other material. E.g. InAs/GaSb.

Type III band alignment shows in Fig. 3.3.

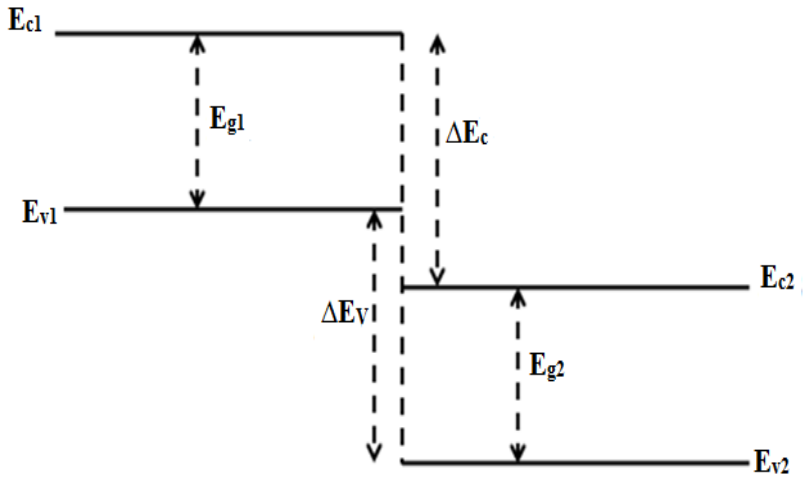


Fig. 3.3 Type III Broken gapalignment

### 3.3 Energy Band Diagram of Heterostructure between two semiconductors :

Assuming that the two semiconductors 1 and 2 have the band gaps of $E_{g1}$ and $E_{g2}$ with $E_{g2} > E_{g1}$, electron affinities of $\chi_1$ and $\chi_2$, work functions of $\phi_1$ and $\phi_2$, doping densities of $N_1$ and $N_2$, dielectric constants of $\varepsilon_1$ and $\varepsilon_2$ respectively. The work function and electron affinity can be defined as:

**Work function ($\phi_m$)** = defined as that energy required to remove electron from the Fermi level ($E_F$) to the outside the material i.e. vacuum level.

**Electron affinity ($\chi$)**= are defined as that energy required to remove electron from the bottom of the conduction band ($E_C$) to the outside the material i.e. vacuum level.

Among three type of the heterostructures mentioned above, the most commonly one is the type I heterojunction whose various parameters have been illustrated in terms of the Anderson's model in Fig 3.4.

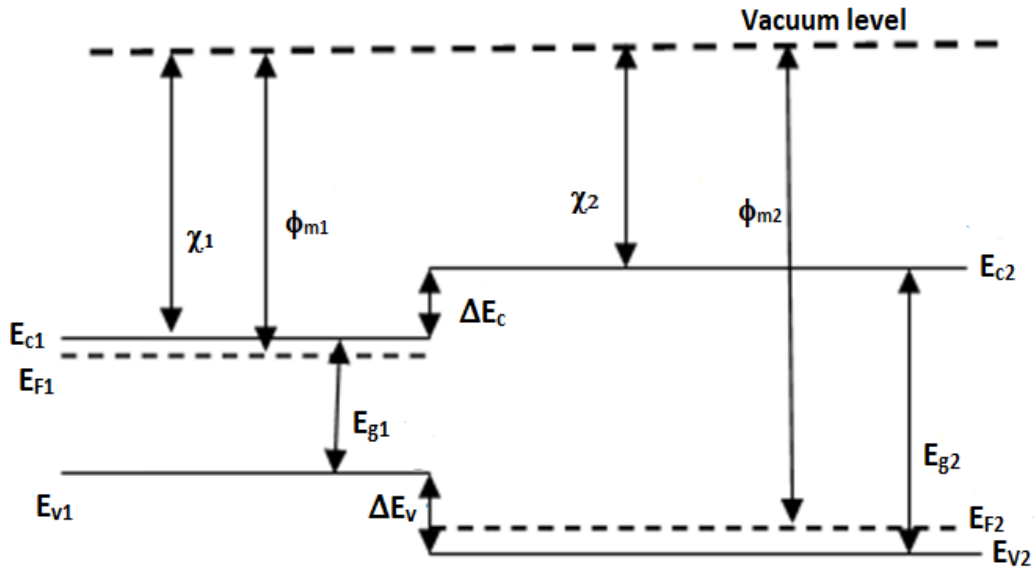


Fig.3.4: Energy-band diagram for two isolated semiconductors with different energy bandgap $E_g$ different work function $q\phi_s$ and different affinities $q\chi$

The difference in energy of the conduction band edges and valance band edges in the semiconductors is represented by $\Delta E_C$ and $\Delta E_V$, respectively and

$$\Delta E_C = \chi_1 - \chi_2 \qquad (3.1)$$

$$\Delta E_V = (E_{g2} - E_{g1}) \pm \Delta E_C \qquad (3.2)$$

In Eq.3.1, the negative sign for $\Delta E_C$ is used for type I and positive sign used for the type II alignment heterojunctions. According to the sign convention used for $\Delta E_V$, positive value suggests that the energy of the valence band of semiconductor 1 is higher than that of semiconductor 2. Although, the Anderson's model can be used successfully for roughly predicting the band discontinuities of many heterojunctions, however, the I-V characteristics of the heterojunctions derived based on the this model usually do not agree with the experimental results. This is due to the impractical assumptions of abrupt metallurgical junctions and the absence of any interface states in the Anderson's model.

## 3.4 Band Diagram of $MoS_2$/p-Si heterojunction diode:

In this work, a heterojunction is formed between n-$MoS_2$ thin film and p-Si substrates; the bandgap of $MoS_2$ is calculated from UV-Vis spectrum and bandgap of Si is standard and well-reported in the literature

$E_{g1}$ (band gap of $MoS_2$) = 3.85 eV [from UV-Vis spectrum]

$E_{g2}$ (band gap of Si) = 1.1 eV

$\chi_1$ (Electron affinity of $MoS_2$) = 4.2 eV

$\chi_2$ (Electron affinity of Si) = 4.05 eV

Based on the above details, the band diagram of n-$MoS_2$/p-Si heterojunction is formed. The Fig. 3.5 (a) Shows the energy band diagram of $MoS_2$/-Si heterojunction before equilibrium and Fig. 3.5 (b) is energy band diagram of $MoS_2$/-Si heterojunction after thermal equilibrium reached. Based on above information, the value of $\Delta E_c$ and $\Delta E_v$ is calculated and given as:

$\Delta E_c$ = 0.15 eV

$\Delta E_v$ = 2.90 eV

**Before Thermal Equilibrium:**

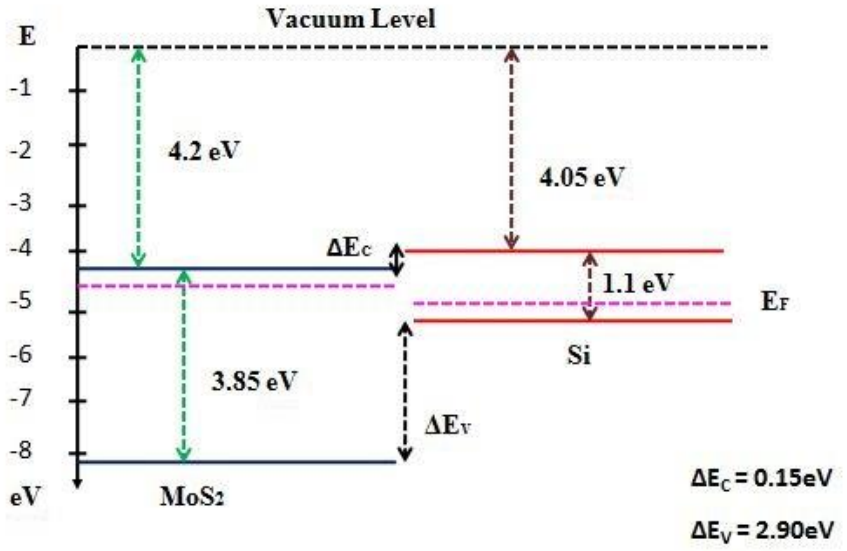


**(a)**

**After Thermal Equilibrium :**

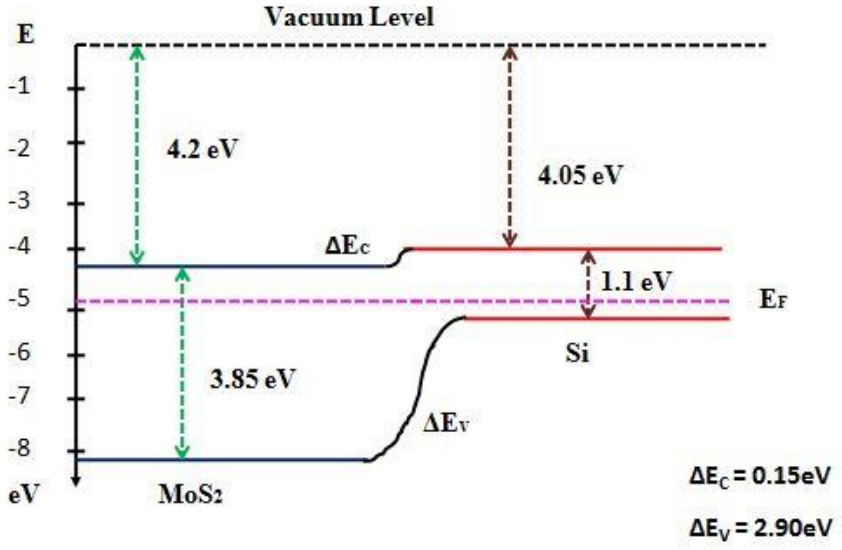


**(b)**

Fig. 3.5: Energy band diagram of $MoS_2$/-Si heterojunction (a) before (b) after thermal equilibrium

## 3.5 Current transport across Heterostructure Diodes :

The current transfer in metal-semiconductor contacts is mainly due to the main carriers, where the minority carriers are responsible, in contrast to p-n junctions. Fig.3.6 shows four basic transport processes under forward bias and the processes of reverse bias are vice versa. The four transport processes across the junction is given as:

**(1)** Electrons are transport from the semiconductor over the potential barrier into the metal,

**(2)** Quantum-mechanical tunnelling of electrons through the barrier and it is vital for highly doped semiconductors and it is responsible for most ohmic contacts,

**(3)** Recombination in the space-charge region. It is identical to the recombination process during the injection of a p-n junction.

**(4)** Hole injection from the metal to the semiconductor and is equivalent to recombination in the neutral region.

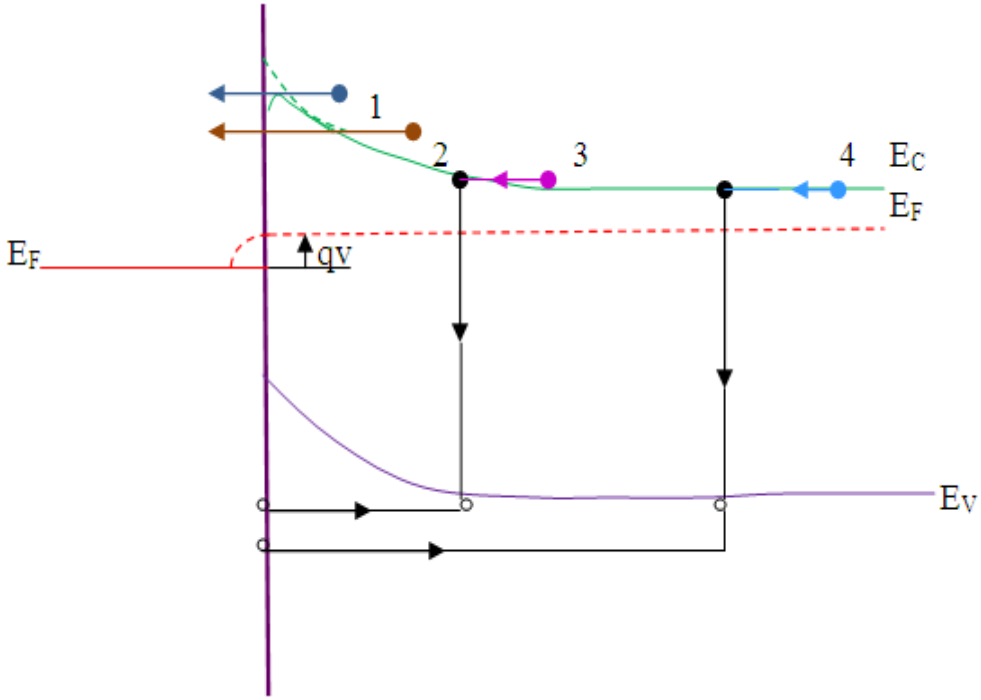


Fig. 3.6: Four basic transport processes under forward bias

### 3.5.1 Current-Voltage (I-V) characteristics based on Thermal Emission Theory:

The thermionic emission theory by Bethe is derived from the assumptions that

(i) The barrier height ($q\phi_B$) is much greater than KT, $q\phi_B\,(=q(\phi_m-\chi_s)) >> kT$

(ii) Thermal equilibrium is recognized at the plane that calculate the emission, and

(iii) One can superimpose two current fluxes – one from metal to semiconductor, the other from semiconductor to metal because the existence of a total current flow and it does not affect this equilibrium, each with a different imref.

Based on these assumptions, the current density $J_{s\to m}$ from the semiconductor to metal is given by the concentration of electrons with energies sufficient to overcome the potential barrier and traversing in the x direction:

$$J_{s\to m} = \int_{E_F+q\phi_B}^{\infty} qv_x\,dn \tag{3.3}$$

Where, $E_F + q\phi_B$ is the minimum energy required for thermionic emission into the metal, and $v_x$ is the carrier velocity in the direction of transport. The final expression for the current density at the metal-semiconductor junction of the Schottky diodes can be written as based on the calculation as discussed in the following ref [Sze (1981)]

$$J = \left[A^* T^2 \exp\left(-\frac{q\phi_{B,eff}}{kT}\right)\right]\left[\exp\left(\frac{qV}{\eta kT}\right)-1\right] \tag{3.4}$$

where

$$J_S = A^* T^2 \exp\left(-\frac{q\phi_{B,eff}}{kT}\right) \tag{3.5}$$

is the reverse saturation current density, $\phi_{B,eff} = V_n + V_{bi}$ is the barrier height, $V_n = E_C - E_F$ in the neutral region of the semiconductor, $V_{bi}$ is the built-in potential, $\eta$ is the ideality factor of the Schottky junction, and

$$A^* = \frac{4\pi q m_e^* k^2}{h^3} \tag{3.6}$$

is the effective ***Richardson constant*** for thermionic emission of electron over the Schottky barrier where $m_e^*$ is the effective density of mass of electrons in the semiconductor, $k$ is the Boltzmann constant and $h$ is the Plank's constant. For $MoS_2$, the Richardson constant is 54 $Acm^{-2} K^{-2}$[54].

### 3.5.2 Determination of reverse saturation current, barrier height and ideality factor

For moderately doped semiconductors, the forward biased I-V characteristics can be approximately obtained from $V > \frac{3kT}{q}$ as

$$I = I_S\left[exp\left(\frac{qV}{\eta kT}\right) - 1\right] \approx I_S\, exp\left(\frac{qV}{\eta kT}\right) \tag{3.7}$$

Taking natural logarithm in both sides of Eq. (3.7), we can write

$$ln(I) = ln(I_S) + \frac{qV}{\eta kT} \tag{3.8}$$

It is observed from Eq.(3.8) that the saturation current $I_S$ can be determined by extrapolating the current from the log-linear region to $V = 0$. Since $I_S$ is constant for a particular device, the ideality factor can be obtained by differentiating Eq. (3.8) with respect to *V* as

$$\eta = \frac{q}{kT}\frac{\partial V}{\partial \ln(I)} \tag{3.9}$$

Eq. (3.9) clearly shows that the ideality factor can be determined from the slope of the ln (*I*) versus *V* plot.

Once the reverse saturation current density is known, the effective barrier height can be written as

$$\phi_{B,eff} = \frac{kT}{q} ln\left(\frac{AA^* T^2}{I_s}\right) \tag{3.10}$$

## 3.6 Capacitance-Voltage (C-V) Characteristics:

The space-charge region width dependent on voltage lies at the main part of the C–V technique.

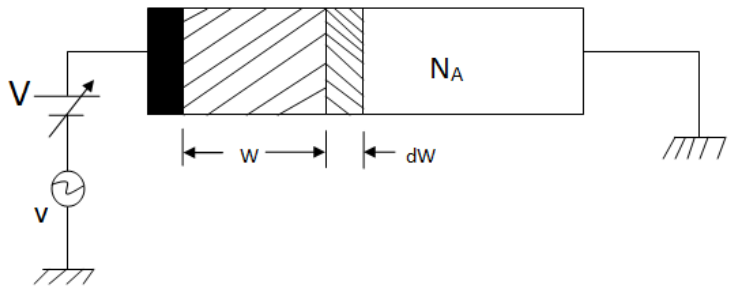


Fig. 3.7 A reverse-biased Schottky diode

We consider the Schottky barrier diode of Fig. 3.7. The semiconductor is p-type with doping density $N_A$. A dc bias V produces a space-charge region of width W. The differential or small signal capacitance is defined by

$$C = \frac{dQ_m}{dV} = -\frac{dQ_s}{dV} \tag{3.11}$$

Where, $Q_m$ and $Q_s$ are the metal and semiconductor charges. The negative sign accounts for negative charge in the semiconductor SCR (negatively charged ionized acceptors) for positive voltage on the metal for reverse bias. The capacitance is determined by the application of a small amplitude ac voltage to dc voltage. C-V measurements are commonly used for electrical characterization of Schottky as well as heterojunction diodes and of the semiconductor material itself. As we know that the depletion region of the Schottky contact entirely lies within the semiconductor and consists of space charge region with ionized donors which are largely unscreened by mobile carriers. The depletion region thus forms a “parallel plate like” capacitor with the metal and the undepleted bulk of the semiconductor as the two plates and the depletion width as the distance between the two plates Since, the width of the depletion region $(W_d)$ is changed with an applied external bias voltage (V) to the Schottky junction, the capacitor is also expected to change with the bias voltage. The expression for the bias voltage dependent depletion region of the metal and n-type semiconductor based Schottky junction device can be given by

$$W_d = \sqrt{\frac{2\varepsilon_s \varepsilon_0}{qN_D}\left(V_{bi} - \frac{kT}{q} - V\right)} \tag{3.12}$$

Where, $N_D$ and $\varepsilon_s$ are the donor concentration and the relative dielectric constant of the semiconductor respectively and $\varepsilon_0$ is the permittivity of the free space. The total space charge $Q_{sc}$ in the depletion region is given by

$$Q_{sc} = qN_D W_d A \tag{3.13}$$

Where, $A$ is the area of the contact. The small-signal capacitance of the Schottky junction is then given by

$$C = \frac{dQ_{sc}}{dV} = A\sqrt{\frac{q\varepsilon_s \varepsilon_0 N_D}{2\left(V_{bi} - \frac{kT}{q} - V\right)}} \tag{3.14}$$

This can also be written as:

$$\frac{A^2}{C^2} = \left(\frac{2}{q\varepsilon_s \varepsilon_0 N_D}\right)\left(V_{bi} - \frac{kT}{q} - V\right) \tag{3.15}$$

Clearly, if the measured values of $A^2/C^2$ is plotted as a function of the applied bias voltage "*V*" by applying a small a. c signal, we will get a straight line whose slope can give the effective donor concentration of the semiconductor described by

$$N_D = -\frac{2}{q\varepsilon_s \varepsilon_0 A^2}\left[\frac{d}{dV}\left(1/C^2\right)\right]^{-1} \tag{3.16}$$

Further, the built-in voltage $V_{bi}$ can be obtained from the intercept of the slope with the $A^2/C^2$ axis. Once the $V_{bi}$ is determined, the barrier height can also be estimated as $\phi_{B,eff} = V_n + V_{bi}$.

# CHAPTER 4

# SYNTHESIS AND CHARACTERIZATION OF $MOS_2$ QUANTUM DOTS ($QD_S$) ON p-Si SUBSTRATES

## 4.1 Introduction :

$MoS_2$ is a 2D semiconductor material with unique electronic and optoelectronic properties. It is observed from the literature that $MoS_2$ with small planar dimensions exhibit excitation dependent PL with wavelengths in the range of 400–600 nm which have various applications especially for multi-colour light emitting diodes (LEDs) [8, 48, 55]. Therefore, high quality and large-scale synthesis of $MoS_2$ nanostructure is essential to manufacture various electronic devices. It may be mentioned here when size of $MoS_2$ reduced less than 10 nm, the bandgap of $MoS_2$ is further broadened because of the effect of quantum confinement (QCE) and $MoS_2$ exhibit and new size-dependent properties. Different top-down and bottom-up techniques have been reported in the literature to obtain nanostructures of $MoS_2$, however, in this work we are using a simple and cost-effect facile colloidal synthesis approach.

## 4.2 Cleaning of the substrates (Si + Glass) :

- **Silicon Wafer :**

In this experiment, I have used boron doped p-Si wafer (100) of thickness 380 μm (4") purchased from the **TED PELLA, INC**. as a substrate. The de-ionised (DI) water ($\rho$ = 18 MΩ-cm) obtained from Milli-Q water plant (Millipore, USA). First, I have taken a p-type silicon wafer and divided this wafer with small pieces by using diamond cutter. Now, the pieces of Si wafer were immersed in acetone for 15-20 minutes for removal of any dust particles and contaminations. After this wafers were rinsed by the DI water and then further immersed in the Iso-propanol for 15-20 minutes. Again, wafers are rinsed in DI water followed by dipped in the solution of 10:1

($H_2O$:HF) for 10 minutes for striping of native oxide layer . Finally, wafer pieces rinsed in DI water and then it is dry at room temperature for further use.

- **Glass :**

I have taken a 75 mm long × 25 mm wide glass-slide purchased from *Blue Star Micro slides and cover glass* of thickness 1.35 mm. This glass slide is equally divided by diamond cutter. Each glass pieces is properly cleaning for removing dust particles from glass surface. In the process, firstly, glass pieces are cleaning with bio-chemical solution and after that cleaning with DI water. Secondly, these are immersing with acetone for 15-20 minutes and after that cleaning with DI water. Thirdly, these are immersing with iso-propanol for 15-20 minutes and after that cleaning with DI water. At last, all pieces of glass are dipping with 10 HF solutions for 10 minutes and cleaning with DI water and then all pieces of glass are dry at room temperature.

## 4.3 Experimental Section :

### 4.3.1 Materials :

Ammonium tetrathiomolybdate ($(NH_4)_2MoS_4$), Oleic acid (OA), oleylamine (OLA) were purchased from Sigma-Aldrich, 1-octadecene (ODE) was purchased from Alfa Aesar and Acetone, Chloroform, Iso-propyl alcohol were purchased from GR, Merck. All the chemicals were used without further purification. De-ionized water was used in all experiments.

### 4.3.2 Synthesis of $MoS_2$ QDs :

An effective strategy for the synthesis of nanostructures of $MoS_2$ was developed at the IC centre, Department of Electronics and Tele-communication Engineering, Jadavpur University, Kolkata. $MoS_2$ quantum dots (QDs) were synthesized by a facile colloidal approach. In this process, a mixture of Ammonium tetrathiomolybdate ($(NH_4)_2MoS_4$) (0.013 cc) Oleic acid (OA) (1 ml), Oleylamine (OLA) (3 ml), and 1-octadecene (ODE) (6 ml) heated up to 120$^oC$ for 2.5 h with stirring. The resulting homogeneous solution was switched to a dry nitrogen atmosphere in a muffle furnace (Model No. ENV120T) heated to 250°C slowly and maintained at this temperature for 3 h. After that the temperature of the solution was allowed to cool at room temperature. The resulting $MoS_2$ QDs were precipitated by the addition of acetone, rinsed with

Iso-propanol, and then redispersed in 10 ml of chloroform for further use. The schematic diagram of synthesis of $MoS_2$ QDs is shown in Fig 4.1.

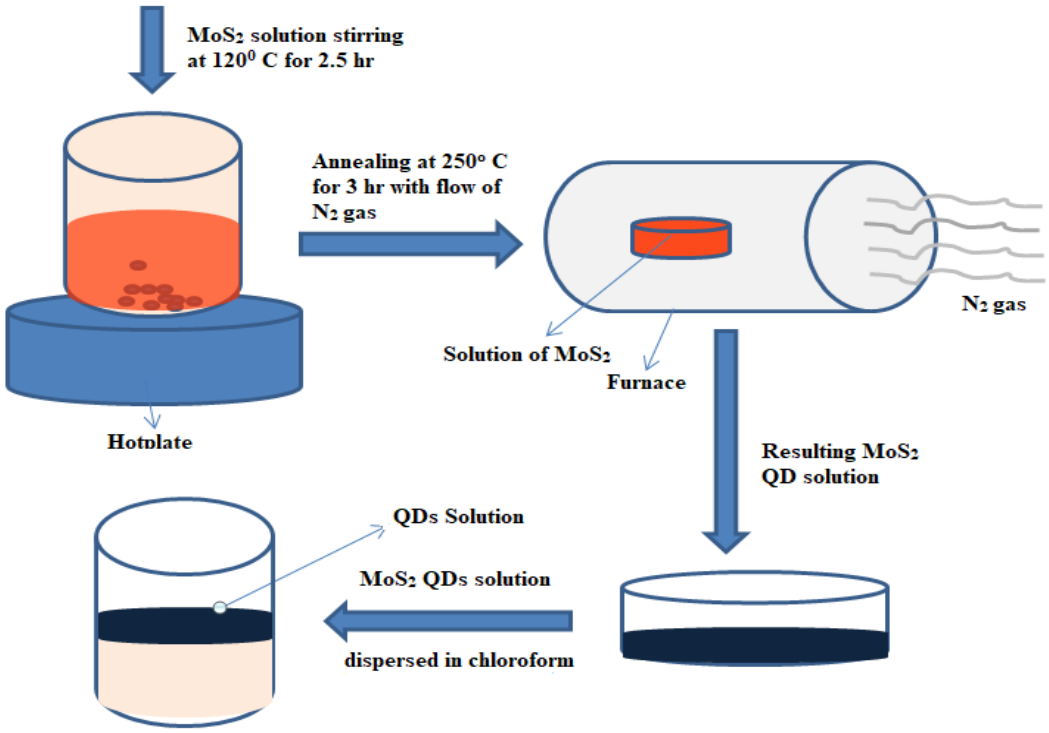


**(a)**


**(b)** **(c)**

Fig: 4.1 (a) Schematic diagram of Colloidal synthesis process for $MoS_2$ Quantum Dots (b) photo image of as-prepared $MoS_2$-QDs solution in a Petridis (c) $MoS_2$ QDs solution dispersed in chloroform for further us

## 4.4 Structural Characterization of $MoS_2$ QDs based thin film:

4.4.1 **Scanning Electron Microscope (SEM) image:** The SEM image of $MoS_2$ thin film coated on p-Si substrates by a typical spin coater (Model No. SCU 2007) with rpm 3000 in 20sec.

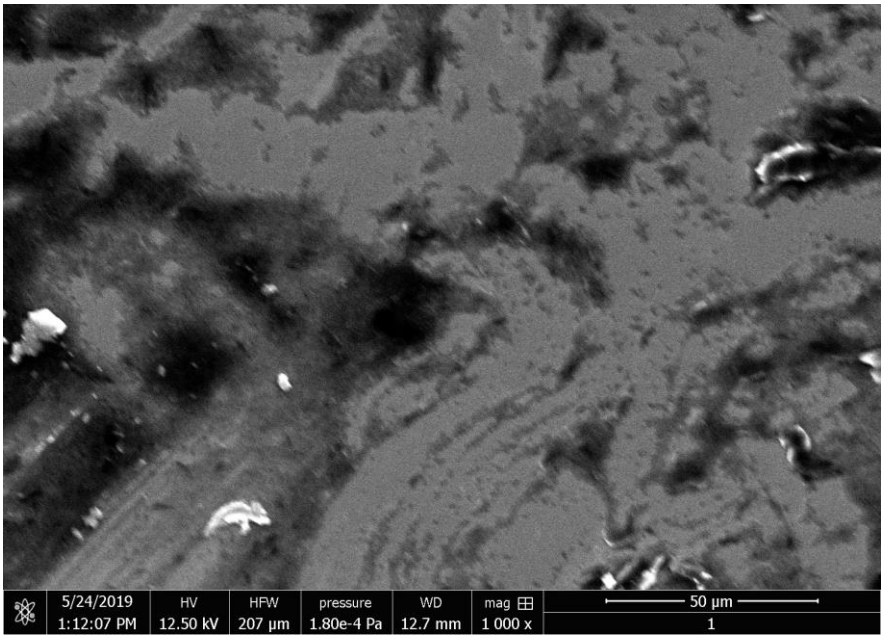


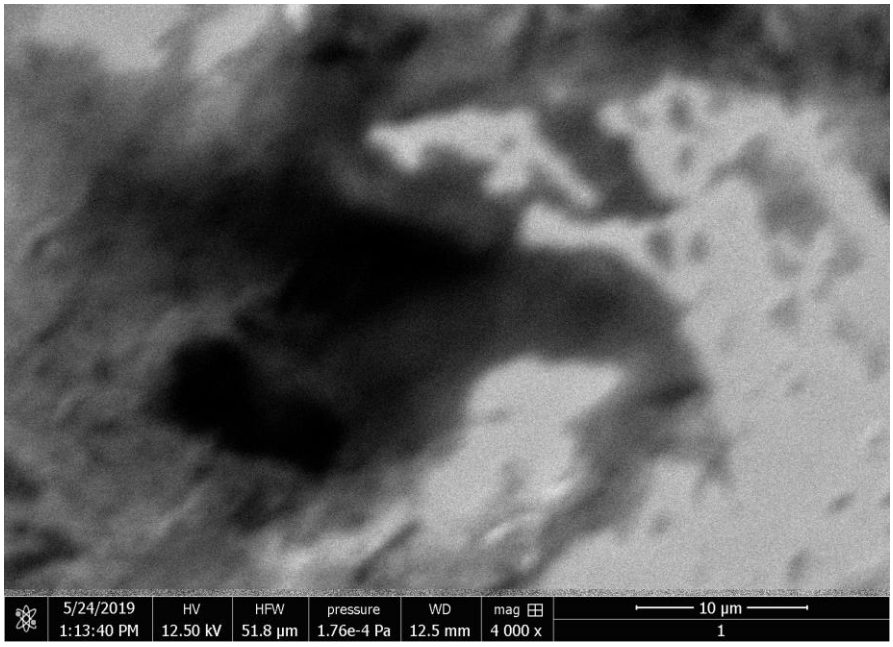


Fig.4.2 SEM image of $MoS_2$ QDs coated thin film on Si substrate

## 4.5 Optical Characterization of $MoS_2$ QDs:

The as-prepared $MoS_2$ QDs are analysed by optical characterization technique such as room temperature and excitation wavelength dependent PL spectra and UV-Visible spectrum.

### 4.5.1 Photoluminescence Spectra (PL) :

The PL spectrum (**Omni PL**) of $MoS_2$ QD based thin film coated on Si substrates is shown in Fig.4.3. All the PL spectra mentioned in this thesis recorded at room temperature. For PL measurements, we used a 532 nm solid state laser of to excite $MoS_2$ film coated on the Si substrates. It may recall here from chapter 1, that due to the transition from indirect to direct bandgap, $MoS_2$ nanostructures show good luminescence properties (as contrast to bulk $MoS_2$, no Pl is observed due to indirect band gap of materials). The observation of good PL (as shown in Fig.4.3), shows that as-synthesised nanostructure of $MoS_2$ have direct band gap with peak intensity at 574 nm when excited with laser light of 380 nm. This result also matched with previous study in the literature for $MoS_2$ quantum dots [46], [56],[47, 57].

Fig: 4.3 PL peaks of $MoS_2$ QDs for single excitation coated on silicon substrate

The PL spectra of $MoS_2$ QDs based thin film coated on Si substrates were measured under various excitation wavelengths, as shown in Fig. 4.4. It shows that with the increase in the excitation

wavelength from 360 nm to 480 nm, the emission peak shifts to the red and its intensity decreases rapidly over emission wavelengths ranging from nearly 560 nm to 750 nm. Excitation dependent PL indicates polydispersity of the $MoS_2$ QDs dispersions, which is characteristic of the colloidal synthesis method in consistent with previous reports[46]. The phenomenon is recognizing to the PL from the *K* point of the Brillouin zone as we have already seen in the band structure of monolayer $MoS_2$ (Fig. 1.4 (a)). The other reason for the excitation dependent Pl is the defect level formation after oxygen adsorbed to the particle edges. [58]. Excitation dependent PL behaviour is useful in multicolour imaging applications [59]. As reported in the literature, the size of QDs decreases with the increasing emission peak energy, in good agreement with the effect of Quantum confinement [47].

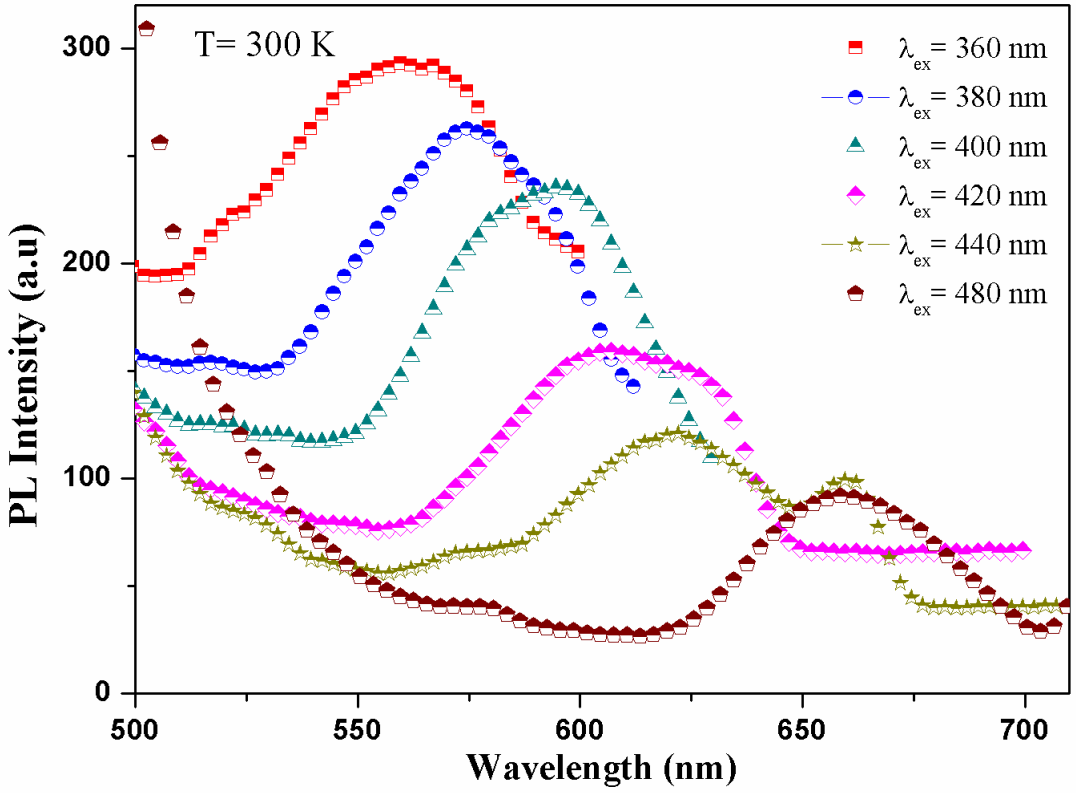


Fig.4.4 Excitation wavelength dependent PL spectra of $MoS_2$ QDs coated thin film on Si substrates with wavelength varies from 360 nm to 480 nm

The schematic diagram of the Quantum dot size effect with emission and excitation wavelength is shown in Fig. 4.6 which is reproduced from the Ref.[8]. The variation of peak position with

variable excitation wavelength was demonstrated in Fig.4.6 by extracting the representative PL peak locations from Fig.4.4 respectively. It exhibited an excitation-wavelength linearly dependent PL behaviour in $MoS_2$ QDs, which is consistent to the previous results observed literature [8, 55].

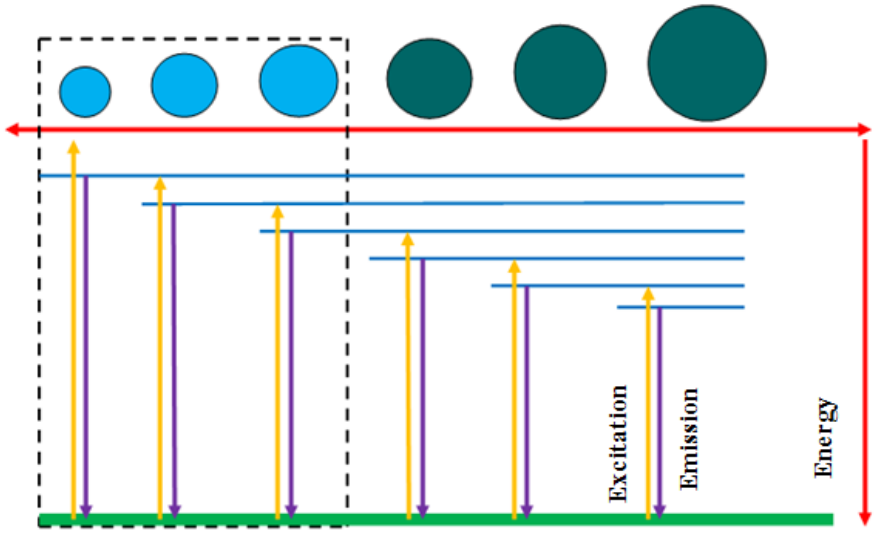


Fig. 4.5 Schematic diagram of the size effect in QDs materials

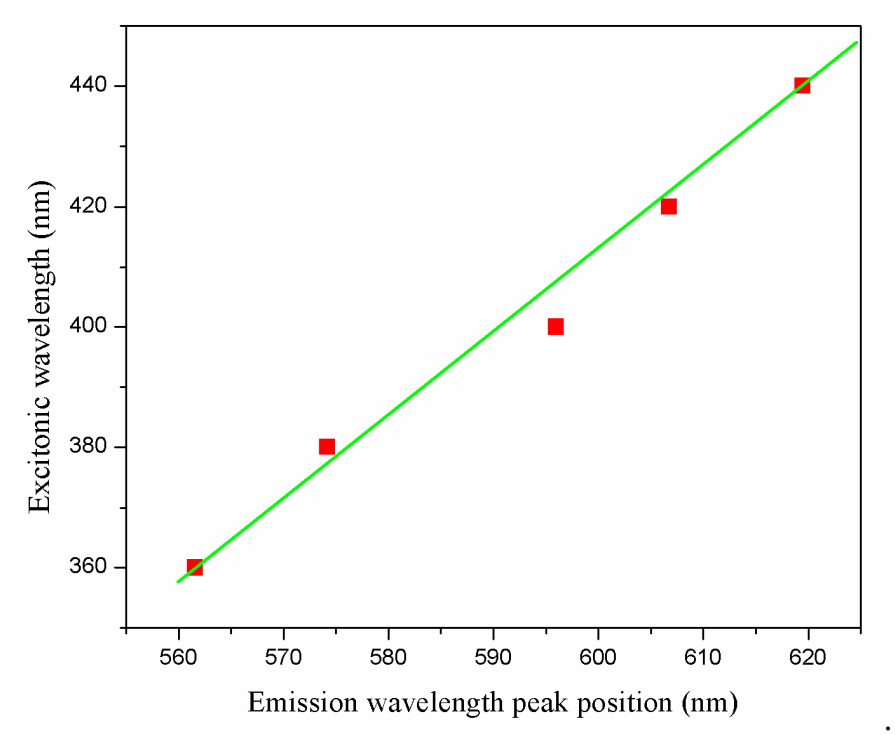


Fig. 4.6 Monitored emission peak wavelength versus excitonic wavelength

### 4.5.2 UV-Visible spectrum:

The UV-vis spectrum of as-prepared $MoS_2$ QDs based thin film coated on glass substrates is shown in Fig. 4.8(a). In general, bulk $MoS_2$ has four characteristics optical absorption peaks at wavelength corresponding to 340, 430, 590, and 650 nm respectively [48, 60]. However, It has been observed that the optical absorption of zero dimensional $MoS_2$ exhibits a strong blue-shift when the dimensions of the $MoS_2$nanostructures are reduced to less than 50 nm, because the quantum confinement effect as reported in the literature[8, 48, 60].In this work, absorption spectra of as-prepared $MoS_2$ QDs shows only one peak in the near-UV region with wavelength< 300 nm which is typical excitonic features of $MoS_2$-QDs[48].

In order to find the value of bandgap, by using the following relation

$$\alpha h\gamma = A(h\gamma - E_g)^m \tag{4.1}$$

Where $\alpha$ is absorption coefficient, $h\gamma$ is the photon energy, (value of $h = 6.634\times10^{-34}\ j-\sec$), m = ½ (for direct allowed transitions)

$$h\gamma = h.\left(\frac{c}{\lambda}\right) \tag{4.2}$$

Where c is the velocity of light and λ is the wavelength. By plotting the graph between square of absorption energy $(\alpha h\gamma)^2$ vs. $h\gamma$ the band gap of as-prepared of $MoS_2$-QDs can be calculated as 3.88 eV.It is well known that the bandgap of a semiconductor increases when its size of the nanostructureapproaches the excitonic Bohr radius which isabout 2.0 nm for $MoS_2$[8], therefore it is valid to consider the QCE for of size less than tens of nanometers.

The bandgap can be derived by the following equation[8]:

$$E^* = E_g + \frac{h^2}{8\mu r^2} - \frac{1.8e^2}{4\varepsilon_0\varepsilon_r} \tag{4.3}$$

The μ is the reduced mass of exciton (0.16mo, where $m_o$ is the free-electron mass), h is the Plank's constant, $E_g$ is 1.29 eV ($MoS_2$ indirect band gap),and the dielectric constant is about 6.8[8]. According to the size distribution, the distribution of bandgap can be obtained (Fig. 4.7(a)) and the most probable bandgap is estimated to be 3.8 eV (bulk bandgap of 1.29 eV) which is closed match with our experimental observation of 3.88 eV from UV-vis spectrum.

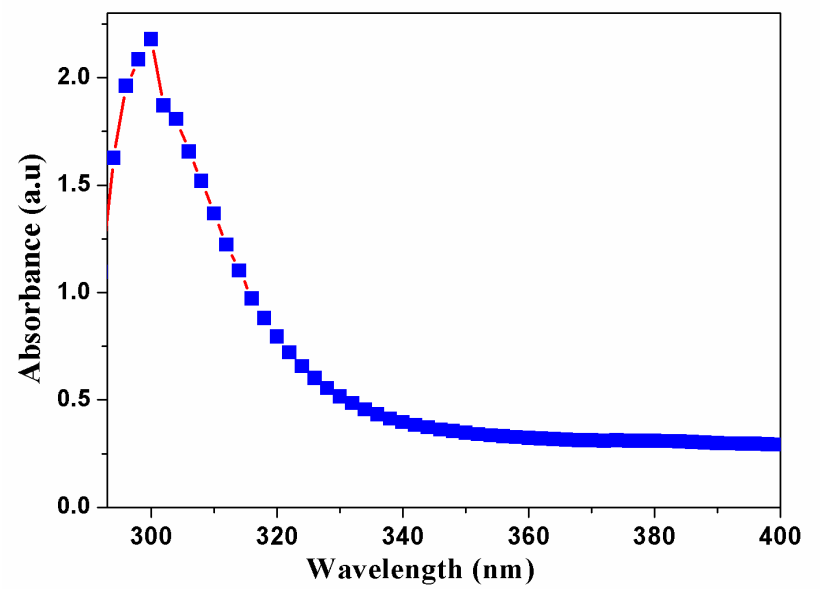


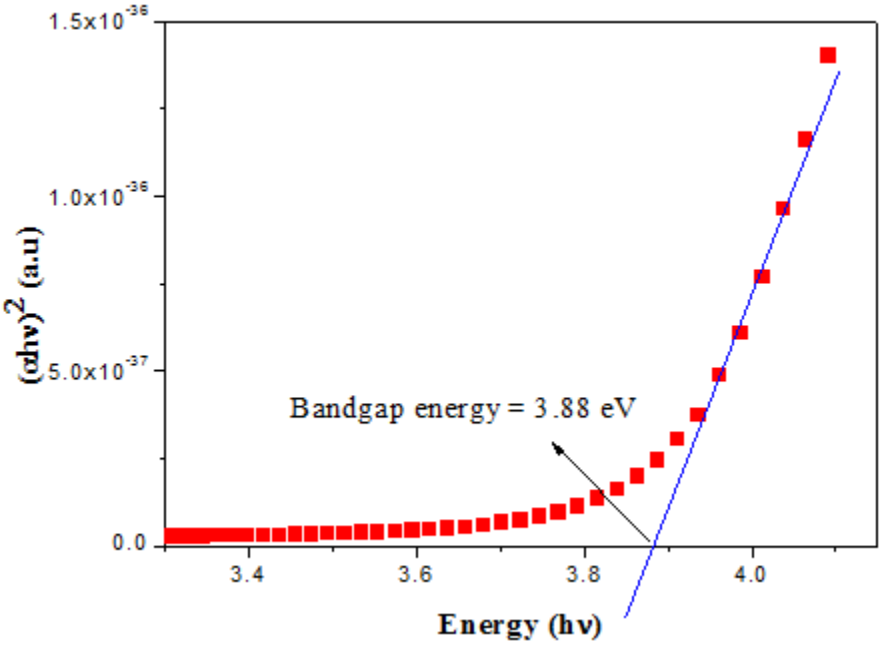


Fig: 4.7 (a) Absorption spectra (b) Band gap calculations of $MoS_2$ QDs based thin film coated on glass substrates

# CHAPTER 5

# ELECTRICAL CHARACTERISTICS OF n-$MOS_2$/p-Si HETEROJUNCTION DIODES

## 5.1 Introduction

The present chapter deals with the fabrication and characterization of Al/Ti/n-$MoS_2$/p-Si/Al/Ti heterostructure diode. The metal contacts of Al/Ti contacts on both sides of n-$MoS_2$ as well as p-Si substrates have been deposited by using thermal evaporation method. The thermal evaporation is one of the most widely used techniques of physical vapor deposition (PVD). In this method, the source material is evaporated in a vacuum closed chamber and vacuum allows vapor particles to travel directly to the target object (substrate) where they condense back to a solid state as sc. The source materials to be evaporated are placed on the heated semimetal (ceramic) evaporators, known as "boats" due to their shape. The materials are first melted in the boat cavity due to heat and are then evaporated in a high vacuum environment into a cloud above the source. The substrate (i.e. target) on which the deposition has to be performed is placed at a certain distance from the source (i.e. boat). The evaporated particles can travel directly to the deposition target without colliding with the background gas in the high vacuum environment. It may be mentioned that hot objects (e.g. the heating filaments) in the evaporation chamber may produce unwanted vapors which can degrade the quality of the vacuum in the chamber to some extent. The thickness of the as-deposited thin films of the desired material can be monitored by a quartz crystal micro-balance attached with the thermal evaporation unit.

In this chapter, the electrical characteristics of n-$MoS_2$/p-Si heterojunction diodes have been determined by room temperature C-V characteristics and I-V characteristics as discussed in the following sections:

## 5.2 Schematic Structure of the Devices:

The n-$MoS_2$/p-Si based heterojunction diodes were obtained by fabricating the ohmic contacts on both the $MoS_2$ film and back side of the p-Si substrate. The ohmic contact for cathode electrode was fabricated by depositing Al/Ti (~40/70 nm) metal on the $MoS_2$ film side by the shadow mass techniques whereas the anode electrode was achieved by depositing Al/Ti metal (~40/80 nm) on the entire back surface side of the p-Si substrate by the physical vapour deposition technique at a vacuum level of ~$4\times10^{-6}$ mbar. The dots are obtained using shadow masking and the diameter of dot is 2 mm. The effective area of a single Al/Ti dot was $\sim 3.14 \times 10^{-2}$ $cm^2$ and hence a single Al/Ti dot was expected to cover a large number of $MoS_2$ QDs under it. The schematic structure of the n-$MoS_2$/p-Si heterojunction diodes under forward bias operation is shown in Fig. 5.1. Note that the polarities of the source should be reversed for reverse bias operation of the diode. The larger value of the $\Delta E_v$ (2.90 eV) than the $\Delta E_c$ (0.15 eV) (from the chapter 3) prevents the movement of holes from Si to $MoS_2$ [6], [15]. Thus, the current transport in the n-$MoS_2$/p-Si hetrojunction device considered in this study can be determined predominantly by the flow of electrons from the n-$MoS_2$ to the p-Si side of the heterojunction.

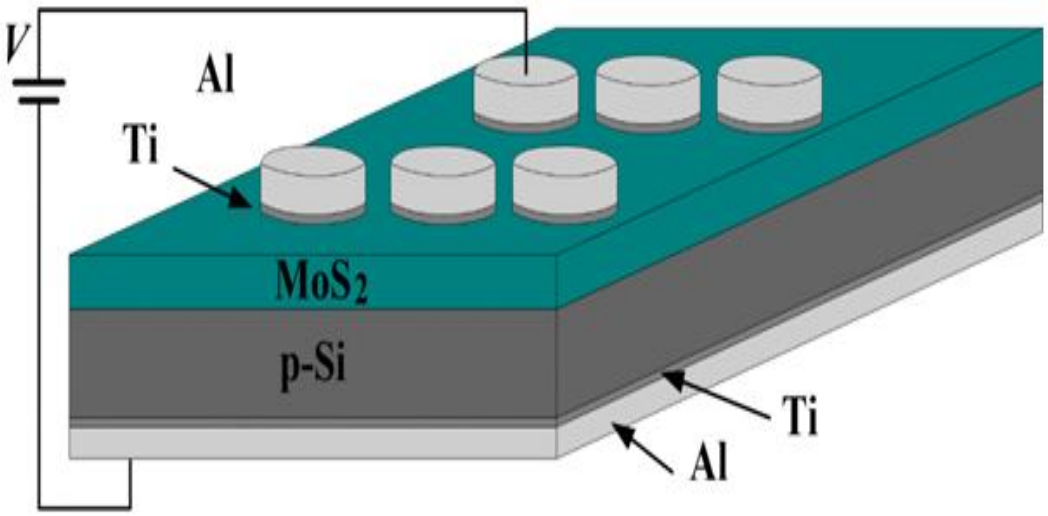


Fig. 5.1 Schematic Structure Device of Al/Ti/p-Si/$MoS_2$/Ti/Al

## 5.3 Analysis of Electrical Characteristics:

### 5.3.1 Capacitance – Voltage (C-V) characteristics:

The C–V characteristics of the n-$MoS_2$/p-Si heterojunction device measured at high frequency of 1 MHz have been shown in Fig. 5.2 with a computer-controlled-impedance analyzer (HP-4284 A, LCR meter) at room temperature. It can be noted that the C–V characteristics of heterojunction devices are extremely sensitive to the low frequencies of the ac signals. However, it turned out that the interface states are almost insensitive to high frequencies ac signals (~1 MHz), and therefore have little effect on the characteristics of the C–V characteristics. In view of the above, the C–V characteristic at only 1-MHz frequency (as shown in Fig. 5.2) is considered in this study. The measured values of C and $A^2/C^2$ for the device considered in the study have been plotted against the applied bias voltage (V) as shown in Fig. 5.2 and Fig. 5.3 respectively.

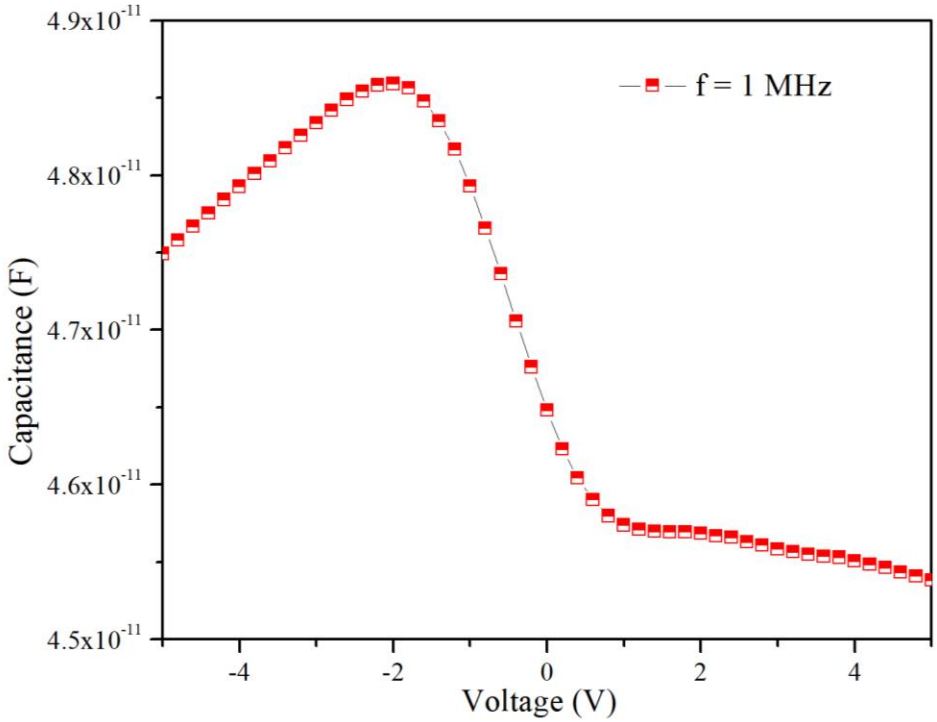


Fig.5.2: Room temperature C–V characteristics of n-$MoS_2$/p-Si heterojunction device.

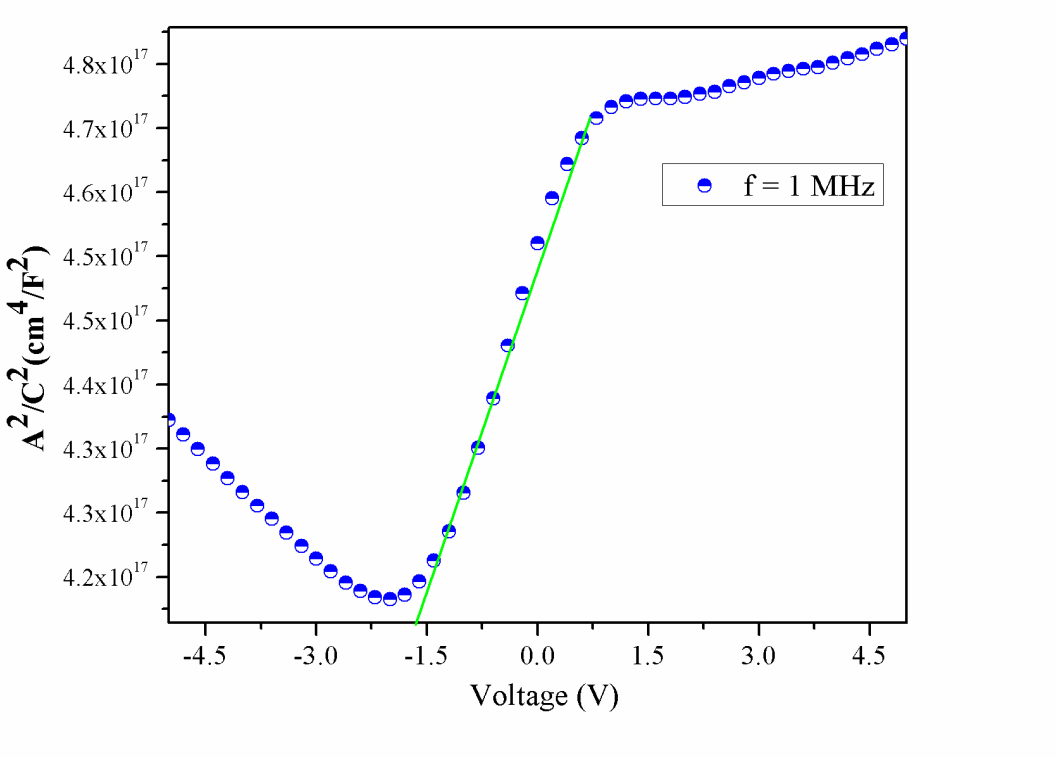


Fig.5.3: $A^2/C^2$ versus V plot for calculation of built- in potential $V_{bi}$ at the junction

The C–V characteristics of n-$MoS_2$/p-Si heterojunction device can be described as follows:

$$\frac{A^2}{C^2} = \frac{2(V_{bi} + V - \frac{KT}{q})}{qN_D\varepsilon_s} \tag{5.1}$$

where C is depletion capacitance, A is the junction area, $N_D$ is the donor density in n-$MoS_2$, $\varepsilon_s$ is the permittivity of the n-$MoS_2$, V is the applied reverse bias voltage, and $V_{bi}$ is the built in potential of the junction.

**(a) Determination of slope:**

Equation (5.1) shows that the $A^2/C^2$ versus V should be a linear curve whose intercept with the applied bias voltage (V) provides the value of $-(V_{bi} - kT/q)$ and slope (say, m) can be used to estimate the doping concentration $N_D$ of $MoS_2$ by using the relation

$$N_D = \frac{2}{mq\varepsilon_s} \tag{5.2}$$

Here, $-(V_{bi} - \frac{KT}{q}) = -1.58$ (Slope from Fig.5. 2)

So, $V_{bi} = (1.58 + 0.026) \sim 1.6$ V (5.3)

Extrapolating the linear segment of the $A^2/C^2$ versus V curve to the applied voltage axis as shown in the Fig., the value of the built-in potential is estimated as $V_{bi} \sim 1.6$ V.

I have calculated the slope (m) value from Fig. 5.4.

$m = 2.50 \times 10^{16}$

$q = 1.603 \times 10^{-19}$

Dielectric constant of $MoS_2 = 6.8$

$\varepsilon_s$ = (permittivity of vacuum × dielectric constant of $MoS_2$)

$= (8.85 \times 10^{-12} \times 6.8)$

$= 60.18 \times 10^{-14}$ F/cm.

$$N_D = \frac{2}{mq\varepsilon_s} = \mathbf{8.326 \times 10^{14}\ cm^{-3}} \tag{5.4}$$

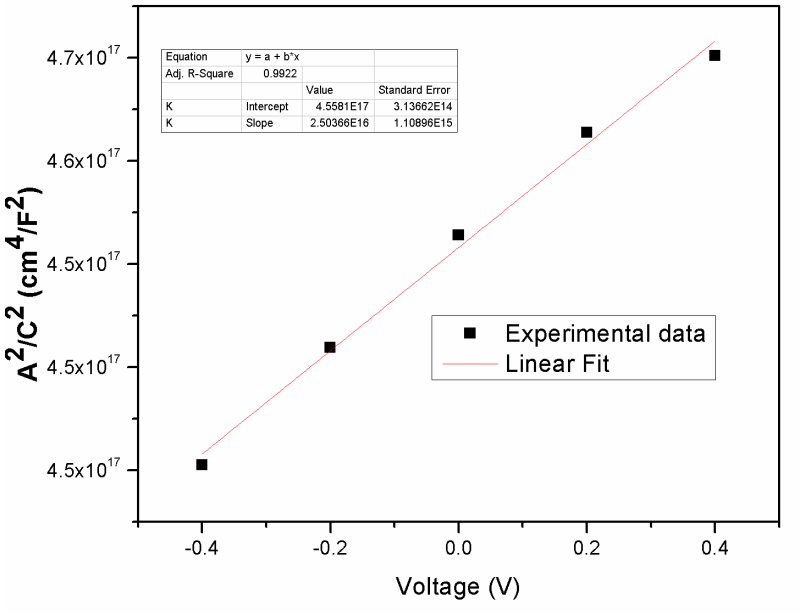


Fig. 5.4 Slope of the $A^2/C^2$ versus V for calculating the m value.

**Barrier Height:**

Now, the value of the barrier height can be estimated by using the relation

$$\phi_{B,eff}^{C-V} = V_{d0} + V_n \tag{5.5}$$

where $V_{d0} = V_{bi} + kT/q$ is the diffusion voltage at zero bias and

$$V_n = \frac{kT}{q} ln\left(\frac{N_C}{N_D}\right) \tag{5.6}$$

$V_{d0}$ is the diffusion voltage at zero bias and $V_n$ represents the depth of Fermi level below the conduction band in neutral region of the semiconductor, where,

$$N_c = \frac{2(2\pi m_e^* kT)^{3/2}}{h^2} \tag{5.7}$$

$N_C$ is the effective density of states in the conduction band with $m_e^* = 0.454m_0$ for $MoS_2$ as the effective mass of the electron of $MoS_2$. The value of Nc can be calculated as $7.5\times10^{18}$ $cm^{-3}$. By putting this value of $V_n = 0.24$ eV determined.

$$V_{d0} = V_{bi} + \frac{KT}{q} = 1.606 + 0.026 = \mathbf{1.632} \tag{5.8}$$

Using (5.3), the barrier height is estimated as ~1.87 eV.

### 5.3.2 Current – Voltage (I-V) characteristics:

The room temperature current (I)-Voltage (V) characteristics of n-$MoS_2$/p-Si have been measured by the semiconductor parameter analyzer (Agilent B1500A) in the voltage range from -2 to +2V as shown in the Fig 5.5. The as-fabricated heterojunction diodes shows a good rectification ratio (i.e. the ratio of the forward current $I_F$ measured at 2V and reverse current $I_R$ at the same reverse bias voltage of –2 V) of $I_F / I_R$ = 7480 under dark condition. According to the

thermionic emission theory, the forward current at the heterojunction can be expressed by the following relation

$$I = I_s[\exp(\frac{qV}{\eta KT}) - 1] \quad (5.9)$$

where $q$ is the elementary charge, $V$ is the applied voltage, $\eta$ is the ideality factor, $k$ is the Boltzmann constant, $I_0$ is the reverse saturation current, $\phi_{B,eff}$ is the effective barrier height (in volt) at zero bias, $A$ is the contact area and $A^*$ is the effective Richardson constant of $MoS_2$ which is equal to 54 A $cm^{-2}$ $K^{-2,}$ $T$ is the absolute temperature,

$\phi_{B,eff}$ is defined as

$$\phi_{B,eff} = \frac{kT}{q}\ln\left(\frac{AA^*T^2}{I_0}\right) \quad (5.10)$$

The value of the reverse saturation current $I_0$ can be calculated from the extrapolated intercept of $ln\, I$ vs. $V$ plot with the current axis for $V = 0$ as discussed in Chapter-1.

**5.3.2.1 Calculation of reverse saturation current, Barrier height, Ideality factor:**

From this fig. 5.6, I have calculated the value of reverse saturation current (Is), Ideality factor and potential barrier height.

**Reverse saturation current (Is):**

Reverse saturation current ($I_s$) is -21.404 (ln value) measured from the graph (Figure 5.5 (b)). The antilog value of $I_s$ is $3.60\times10^{-7}$ A.

**Ideality factor:**

The Ideality factor (η) can be determined by using following relation:

$$\eta = \frac{q}{KT}(\frac{x_2 - x_1}{y_1 - y_2}) \quad (5.11)$$

Here

$X_1 = 0.0416$

$X_2 = 0.1410$

$Y_1 = -21.847$

$Y_2 = -19.890$

From the graph and value of KT/q is 0.026. The calculated ideality factor (η) is 1.95.

**Barrier Height:**

The barrier height can be calculated by using following relation ($\phi_B$),

$$\phi_B = \frac{KT}{q} \ln\left(\frac{A^* T^2}{J_s}\right) \qquad (5.12)$$

Where, $A^*$ is Richardson constant and value of $A^*$ is 54 $A.cm^{-2}.K^{-2}$ of $MoS_2$-QDs. T is 300 K and antilog value of $J_s$ is $1.26 \times 10^{-7}$.

The calculated barrier height ($\phi_B$) value has been obtained as 0.23 eV.

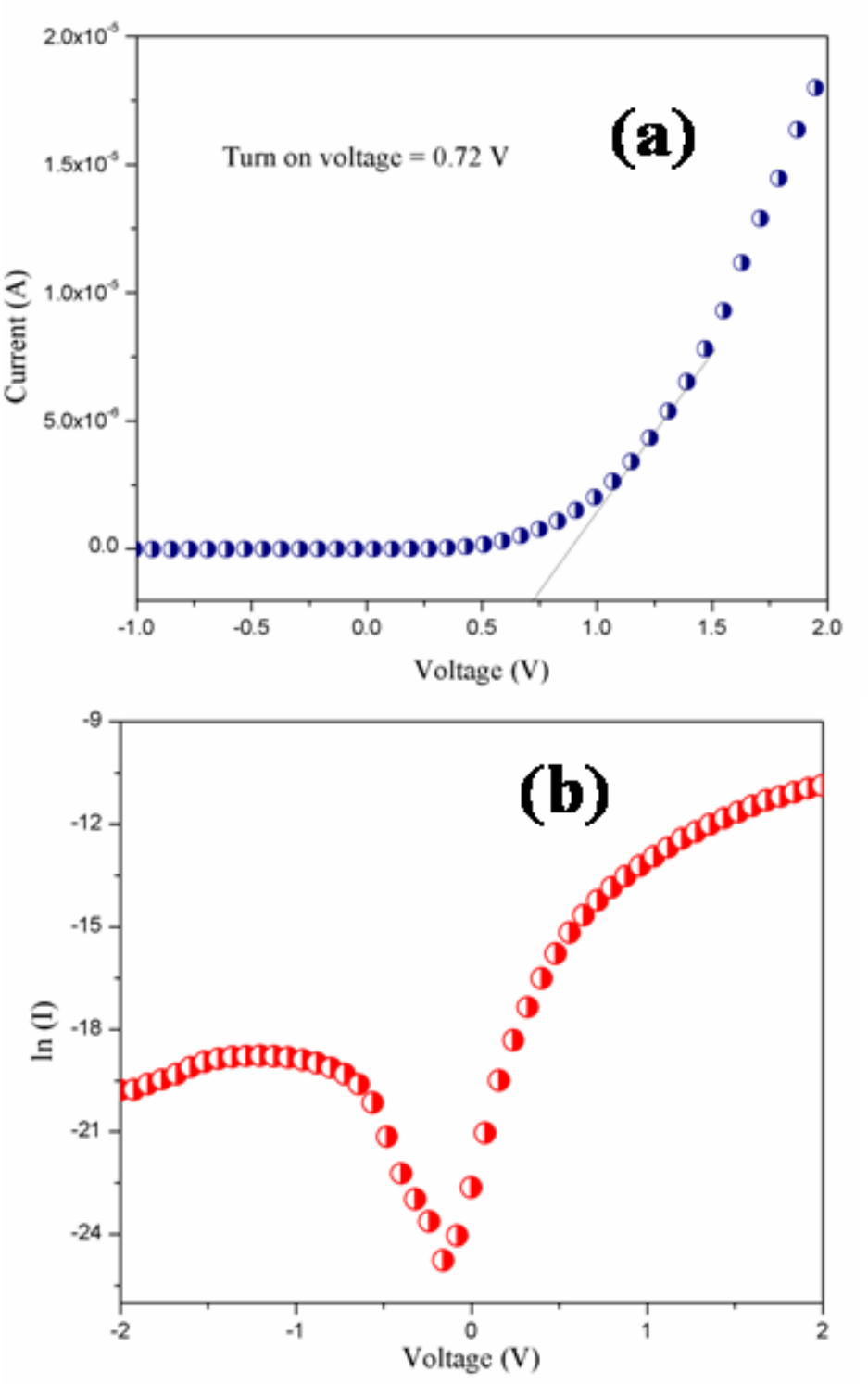


Fig. 5.5: (a) I-V characteristics (b) ln I-V plot of n-$MoS_2$/p-Si device at room temperature

### 5.3.3 Lifetime Measurement of $MoS_2$ QDs

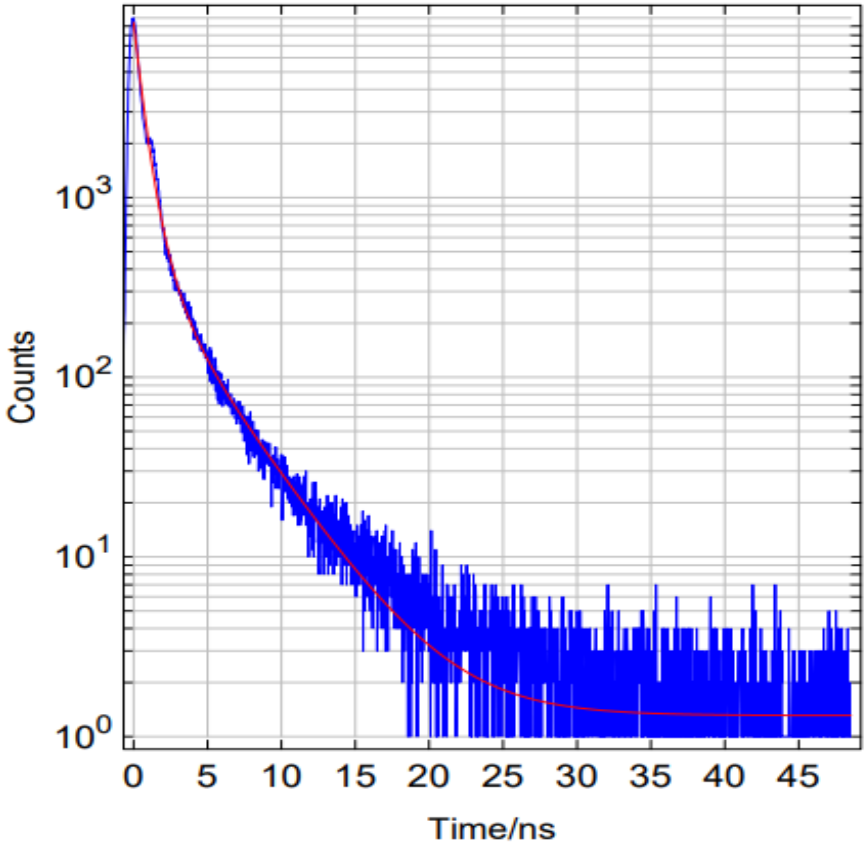


Fig. 5.6 Photoluminescence decay spectra of $MoS_2$-QDs

Fig. 5.6 shows that the typical PL decay spectra of QDs, using the Instrument Response Function (IRF). Experimental data were selected using the Marquardt-Levenberg algorithm for comparison with the lifetime of generated photons with excitation. I have picked up all the spectra which are solid lines with a reasonable exponential attenuation and equation is,

$$I(t) = \int_{-\infty}^{t} IRF(t') \exp\left(-\frac{t-t'}{\tau}\right) \tag{5.13}$$

where τ is the photon-excited carrier life time and the numerical fitting parameter $\chi^2$ value is found to be ~3.524. Exactly chosen exponential decay time shows that only one radiative

recombination of excitons is the existence and insignificant contribution of trap states to $MoS_2$-QDs. The average lifetime of the quantum dots was determined unity with the equation below.

$$\tau = \frac{\sum \alpha_i \tau_i}{\sum \alpha_i} \qquad (5.14)$$

According to the approximation of PL attenuation curve, the calculated average carrier life time turned out to be ~0.75764 ns for QDs. The larger size QDs exhibits a shorter life time and vice versa. Therefore with decreasing diameter, the radiative lifetime becomes more longer. It was found that carriers exciton lifetime of $MoS_2$ QDs of 0.75 ns far exceeds the observed lifetime of complex multi-exponential carriers lifetime for the layered structure of $MoS_2$ [62, 63]. Fig.5.7 shows that all the residuals in $MoS_2$ QDs films are evenly distributed around zero.

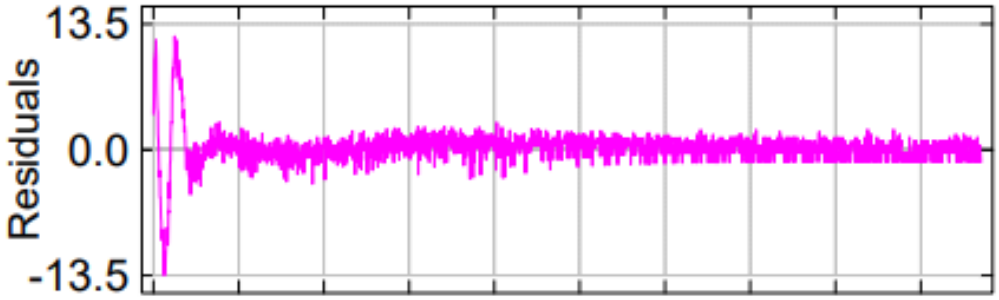


Fig: 5.7: Photoluminescence lifetime of $MoS_2$-QDs of the instrument response function the residuals

# Chapter 6

# Conclusion and Future Scope

## 6.1. Introduction

The basic objective of thesis is to present a detailed analysis of the electrical characteristics of $MoS_2$ QDs based heterojunction devices grown on p-Si substrates. The present chapter has been devoted to summarize and conclude the major observations presented in the various chapters of this thesis. We have also tried to outline some scope for future works related to the areas considered in the present thesis.

## 6.2 Conclusion

$MoS_2$ is one of the most important 2D-TMDCs materials for electronics and optoelectronics application. In this thesis, synthesis of $MoS_2$ QDs carried out by simple facile-colloidal approach and structural and optical characterization done by various techniques. Further, electrical characteristics of n-$MoS_2$/p-Si heterojunction diodes have been investigated by room temperature I-V and C-V characteristics.

**Chapter-1**, presents some general aspects of TMDCs as a 2D material, particularly physical properties of one of the most important 2D-TMDC materials i.e. $MoS_2$ discussed in details.
The band structure of $MoS_2$ with varying number of layers has been analyzed by DFT Theory using Quantum–ATK Software. A direct band gap of 1.81 eV is observed for monolayer $MoS_2$ whereas for bi-layer, tri layer and quad-layer an indirect band gap has been observed which shows suitability of monolayer $MoS_2$ for optoelectronics applications.

**Chapter-2** includes the review of some important state-of-the-art works reported on the electrical characteristics of n-$MoS_2$/p-Si based heterojunction diodes. A detailed literature survey on the reported current-voltage (I-V) and capacitance-voltage (C-V) characteristics of n-$MoS_2$/p-Si heterojunction diodes has been presented.

**In chapter-3**, the band diagram of n-$MoS_2$/p-Si heterojunction diode before thermal equilibrium and after thermal equilibrium has been sketched. By using Anderson model, a conduction band offset of $\Delta E_c$ = 0.15 eV and valance band offset of $\Delta E_v$ = 2.90 eV is calculated.

**In chapter-4,** $MoS_2$ QDs were synthesised by the simple facile colloidal method. The experimental results showed that the resultant QDs had reasonable PL (at 380 nm excitation), and stable dispersion in chloroform as shown in Fig 4.3. The surface characterization of $MoS_2$ QDs based film has been carried out by SEM spectra. The optical characterization of as-synthesised QDs has been carried out by Room temperature PL spectrum, Excitation dependent PL spectra and Raman spectrum. The PL spectrum of $MoS_2$ QDs exhibits a sharp peak at 574 nm at excitation wavelength of 380 nm which is well matched with previous reports in the literature for the same. Excitation dependent wavelength shift observed in the PL spectrum assure that we made $MoS_2$ QDs because wavelength is red shifted with the excitation wavelength via Fig. 4.4. The consistency of the PLE maximum peak position with size distribution confirms that the PL originated from the quantum confinement effects as shown in Fig.4.6. The bandgap of $MoS_2$ film coated on glass substrates have been determined by UV-Vis spectrum.

**In chapter-5,** Al/Ti/n-$MoS_2$QDs/p-Si/Al/Ti heterojunction diode have been fabricated by growing $MoS_2$ QDs based thin film on p-Si substrate. The electrical characteristics of n-$MoS_2$ QDs/p-Si heterojunction diode have investigated in terms of room temperature C–V and I–V characteristics. The barrier height estimated from the C–V measurement is found to be 1.87 eV. The value of $\varphi_{B,eff}$ from I-V is estimated to be 0.23 V at room temperature and $\eta$ is 1.95 . A large difference between barrier height value observed from C-V and I-V observed, this is due presence of large interface defects at n-$MoS_2$/p-Si junction. Time resolved PL studies show the existence of single center of radiative recombination of $MoS_2$ QDs with an excellent carrier life time (0.75 ns) as compared to $MoS_2$ flakes (~10 ps).

## 6.1 Future Scope :

Semiconducting TMDCs materials have been used in many application areas such as photo detector, solar cell, light emitting diodes, sensors, photo transistors etc. In this work, I worked on $MoS_2$ QDs on p-Si substrates. So for future work, I can synthesis $MoS_2$ in different substrates for improving flexibility of the devices for different application. Further, different TMDC materials like as $WS_2$, $WSe_2$ etc can also synthesis for improving light absorption, fluorescence and electroluminescence quantum yields in ultrathin materials. Solution-based methods for preparing and depositing TMDC materials require substantial improvement, especially for high-performance electronic and optoelectronic applications. In particular, the gate tunability of heterostructure devices enables fundamentally different charge transport phenomena. In such heterostructure devices, the spectral photo response can also be tuned with an external gate bias, enabling dynamic tailoring of device characteristics. Since this gate tunability does not exist in bulk semiconductors, devices that exploit it are unlikely to face competition from conventional materials and thus present unimpeded access to new markets. By focusing directly on such unique opportunities, the technological impact of semiconducting TMDCs can likely be maximized.

# References:


1. Jariwala, D., et al., *Emerging Device Applications for Semiconducting Two-Dimensional Transition Metal Dichalcogenides.* ACS Nano, 2014. **8**(2): p. 1102-1120.
2. Gupta, A., T. Sakthivel, and S. Seal, *Recent development in 2D materials beyond graphene.* Progress in Materials Science, 2015. **73**: p. 44-126.
3. Koppens, F.H.L., et al., *Photodetectors based on graphene, other two-dimensional materials and hybrid systems.* Nature Nanotechnology, 2014. **9**: p. 780.
4. Geim, A.K. and K.S. Novoselov, *The rise of graphene.* Nature Materials, 2007. **6**: p. 183.
5. Novoselov, K.S., et al., *Two-dimensional atomic crystals.* Proceedings of the National Academy of Sciences of the United States of America, 2005. **102**(30): p. 10451.
6. Castro Neto, A.H., et al., *The electronic properties of graphene.* Reviews of Modern Physics, 2009. **81**(1): p. 109-162.
7. Bhimanapati, G.R., et al., *Recent Advances in Two-Dimensional Materials beyond Graphene.* ACS Nano, 2015. **9**(12): p. 11509-11539.
8. Gan, Z.X., et al., *Quantum confinement effects across two-dimensional planes in MoS2 quantum dots.* Applied Physics Letters, 2015. **106**(23): p. 233113.
9. Hanbicki, A.T., et al., *Measurement of high exciton binding energy in the monolayer transition-metal dichalcogenides WS2 and WSe2*. Vol. 203. 2014.
10. Yadav, C. and Y. Chauhan, *Modeling of Transition Metal Dichalcogenide Transistors for SPICE Simulation at MOS-AK Workshop, Berkeley, Dec. 2016*. 2016.
11. Bernardi, M., et al., *Optical and Electronic Properties of Two-Dimensional Layered Materials*, in *Nanophotonics*. 2017. p. 479.
12. Han, S.A., R. Bhatia, and S.-W. Kim, *Synthesis, properties and potential applications of two-dimensional transition metal dichalcogenides.* Nano Convergence, 2015. **2**(1): p. 17.
13. Ahmed, S. and J. Yi, *Two-Dimensional Transition Metal Dichalcogenides and Their Charge Carrier Mobilities in Field-Effect Transistors.* Nano-Micro Letters, 2017. **9**(4): p. 50.
14. McDonnell, S.J. and R.M. Wallace, *Atomically-thin layered films for device applications based upon 2D TMDC materials.* Thin Solid Films, 2016. **616**: p. 482-501.

15. Beal, A.R. and W.Y. Liang, *Intercalation studies of some transition metal dichalcogenides.* The Philosophical Magazine: A Journal of Theoretical Experimental and Applied Physics, 1973. **27**(6): p. 1397-1416.
16. Samnakay, R., et al., *Selective chemical vapor sensing with few-layer MoS2 thin-film transistors: Comparison with graphene devices.* Applied Physics Letters, 2015. **106**(2): p. 023115.
17. Zhao, W., et al., *Metastable MoS2: Crystal Structure, Electronic Band Structure, Synthetic Approach and Intriguing Physical Properties.* Chemistry – A European Journal, 2018. **24**(60): p. 15942-15954.
18. Wu, M.-h., et al., *Molybdenum disulfide (MoS2) as a co-catalyst for photocatalytic degradation of organic contaminants: A review.* Process Safety and Environmental Protection, 2018. **118**: p. 40-58.
19. Splendiani, A., et al., *Emerging Photoluminescence in Monolayer MoS2.* Nano Letters, 2010. **10**(4): p. 1271-1275.
20. Nengjie, H., Y. Yujue, and L. Jingbo, *Optoelectronics based on 2D TMDs and heterostructures.* Journal of Semiconductors, 2017. **38**(3): p. 031002.
21. Dong, R. and I. Kuljanishvili, *Review Article: Progress in fabrication of transition metal dichalcogenides heterostructure systems.* Journal of vacuum science and technology. B, Nanotechnology & microelectronics : materials, processing, measurement, & phenomena : JVST B, 2017. **35**(3): p. 030803-030803.
22. Ellis, J.K., M.J. Lucero, and G.E. Scuseria, *The indirect to direct band gap transition in multilayered MoS2 as predicted by screened hybrid density functional theory.* Applied Physics Letters, 2011. **99**(26): p. 261908.
23. Rahman, I.A. and A. Purqon, *First Principles Study of Molybdenum Disulfide Electronic Structure.* Journal of Physics: Conference Series, 2017. **877**: p. 012026.
24. Yang, L., et al., *Properties, Preparation and Applications of Low Dimensional Transition Metal Dichalcogenides.* Nanomaterials (Basel), 2018. **8**(7).
25. Mak, K.F., et al., *Atomically Thin ${\mathrm{MoS}}_{2}$: A New Direct-Gap Semiconductor.* Physical Review Letters, 2010. **105**(13): p. 136805.
26. - Chiu, M.-H., - *Band Alignment Determination of Two-Dimensional Heterojunctions and Their Electronic Applications*.

27. Gusakova, J., et al., *Electronic Properties of Bulk and Monolayer TMDs: Theoretical Study Within DFT Framework (GVJ-2e Method).* physica status solidi (a), 2017. **214**(12): p. 1700218.
28. Mu, C., J. Xiang, and Z. Liu, *Photodetectors based on sensitized two-dimensional transition metal dichalcogenides—A review.* Journal of Materials Research, 2017. **32**(22): p. 4115-4131.
29. Radisavljevic, B., et al., *Single-layer MoS2 transistors.* Nature Nanotechnology, 2011. **6**: p. 147.
30. Huang, C., et al., *Lateral heterojunctions within monolayer MoSe2–WSe2 semiconductors.* Nature Materials, 2014. **13**: p. 1096.
31. Zhang, K., et al., *Interlayer Transition and Infrared Photodetection in Atomically Thin Type-II MoTe2/MoS2 van der Waals Heterostructures.* ACS Nano, 2016. **10**(3): p. 3852-3858.
32. Cheiwchanchamnangij, T. and W.R.L. Lambrecht, *Quasiparticle band structure calculation of monolayer, bilayer, and bulk MoS${}_{2}$.* Physical Review B, 2012. **85**(20): p. 205302.
33. Deng, S., L. Li, and M. Li, *Stability of direct band gap under mechanical strains for monolayer MoS2, MoSe2, WS2 and WSe2.* Physica E: Low-dimensional Systems and Nanostructures, 2018. **101**: p. 44-49.
34. Kuc, A., N. Zibouche, and T. Heine, *Influence of quantum confinement on the electronic structure of the transition metal sulfide $T$S${}_{2}$.* Physical Review B, 2011. **83**(24): p. 245213.
35. Takagahara, T. and K. Takeda, *Theory of the quantum confinement effect on excitons in quantum dots of indirect-gap materials.* Physical Review B, 1992. **46**(23): p. 15578-15581.
36. *Nanocrystals in their prime.* Nature Nanotechnology, 2014. **9**: p. 325.
37. Wise, F.W., *Lead Salt Quantum Dots: the Limit of Strong Quantum Confinement.* Accounts of Chemical Research, 2000. **33**(11): p. 773-780.
38. Bukowski, T.J. and J.H. Simmons, *Quantum Dot Research: Current State and Future Prospects.* Critical Reviews in Solid State and Materials Sciences, 2002. **27**(3-4): p. 119-142.

39. Chukwuocha, E.O., M.C. Onyeaju, and T.S.T. Harry, *Theoretical Studies on the Effect of Confinement on Quantum Dots Using the Brus Equation.* World Journal of Condensed Matter Physics, 2012. **Vol.02No.02**: p. 5.
40. Bera, D., et al., *Quantum Dots and Their Multimodal Applications: A Review.* Materials, 2010. **3**(4): p. 2260-2345.
41. *Photoluminescence Spectroscopy*, in *Characterization of Materials*.
42. Xu, S., D. Li, and P. Wu, *One-Pot, Facile, and Versatile Synthesis of Monolayer MoS2/WS2 Quantum Dots as Bioimaging Probes and Efficient Electrocatalysts for Hydrogen Evolution Reaction.* Advanced Functional Materials, 2015. **25**(7): p. 1127-1136.
43. Loh, G.C., et al., *MoS2 Quantum Dot: Effects of Passivation, Additional Layer, and h-BN Substrate on Its Stability and Electronic Properties.* The Journal of Physical Chemistry C, 2015. **119**(3): p. 1565-1574.
44. Pei, L., et al., *Structural stability, electronic and magnetic properties of MoS2 quantum dots based on the first principles.* Solid State Communications, 2015. **218**: p. 25-30.
45. Wang, Y. and Y. Ni, *Molybdenum Disulfide Quantum Dots as a Photoluminescence Sensing Platform for 2,4,6-Trinitrophenol Detection.* Analytical Chemistry, 2014. **86**(15): p. 7463-7470.
46. Lin, H., et al., *Colloidal synthesis of MoS2 quantum dots: size-dependent tunable photoluminescence and bioimaging.* New Journal of Chemistry, 2015. **39**(11): p. 8492-8497.
47. Mukherjee, S., et al., *Novel Colloidal MoS2 Quantum Dot Heterojunctions on Silicon Platforms for Multifunctional Optoelectronic Devices.* Scientific Reports, 2016. **6**: p. 29016.
48. Li, B., et al., *Preparation of Monolayer MoS2 Quantum Dots using Temporally Shaped Femtosecond Laser Ablation of Bulk MoS2 Targets in Water.* Scientific Reports, 2017. **7**(1): p. 11182.
49. Perumal Veeramalai, C., et al., *Highly flexible memristive devices based on MoS2 quantum dots sandwiched between PMSSQ layers.* Dalton Transactions, 2019. **48**(7): p. 2422-2429.

50. Zhang, X., D. Wu, and H. Geng, *Heterojunctions Based on II-VI Compound Semiconductor One-Dimensional Nanostructures and Their Optoelectronic Applications.* Crystals, 2017. **7**(10): p. 307.
51. Aspnes, D.E., et al., *Optical properties of AlxGa1−x As.* Journal of Applied Physics, 1986. **60**(2): p. 754-767.
52. Anderson, R.L., *Experiments on Ge-GaAs heterojunctions.* Solid-State Electronics, 1962. **5**(5): p. 341-351.
53. Ferreira, R., *Introduction to Semiconductor Heterostructures,* in *Semiconductor Modeling Techniques,* N. Balkan and M. Xavier, Editors. 2012, Springer Berlin Heidelberg: Berlin, Heidelberg. p. 1-17.
54. Lin, Y.-F., et al., *Barrier inhomogeneities at vertically stacked graphene-based heterostructures.* Nanoscale, 2014. **6**(2): p. 795-799.
55. Yin, W., et al., *Multicolor Light-Emitting Diodes with MoS2 Quantum Dots.* Particle & Particle Systems Characterization, 2019. **36**(2): p. 1800362.
56. Pallikkarathodi Mani, N., M. Ganiga, and J. Cyriac, *Synthesis of MoS2 Quantum Dots Uniformly Dispersed on Low Dimensional MoS2 Nanosheets and Unravelling its Multiple Emissive States.* ChemistrySelect, 2017. **2**(21): p. 5942-5949.
57. Liu, C.-W., et al., *Solution processable mixed-solvent exfoliated MoS2 nanosheets for efficient and robust organic light-emitting diodes.* AIP Advances, 2018. **8**(4): p. 045006.
58. Chen, S., et al., *Tuning the optical properties of graphene quantum dots by selective oxidation: a theoretical perspective.* Journal of Materials Chemistry C, 2018. **6**(25): p. 6875-6883.
59. Wang, Z., et al., *One-step and green synthesis of nitrogen-doped carbon quantum dots for multifunctional electronics.* RSC Advances, 2017. **7**(35): p. 21969-21973.
60. Ren, X., et al., *One-step hydrothermal synthesis of monolayer MoS2 quantum dots for highly efficient electrocatalytic hydrogen evolution.* Journal of Materials Chemistry A, 2015. **3**(20): p. 10693-10697.
61. Liu, Y., et al., *MoS2 quantum dots featured fluorescent biosensor for multiple detection of cancer.* RSC Advances, 2017. **7**(86): p. 54638-54643.
62. Korn, T., et al., *Low-temperature photocarrier dynamics in monolayer MoS2.* Applied Physics Letters, 2011. **99**(10): p. 102109.

63. Lagarde, D., et al., *Carrier and Polarization Dynamics in Monolayer ${\mathrm{MoS}}_{2}$.* Physical Review Letters, 2014. **112**(4): p. 047401.